On the Theoretical Analysis of Network-Wide Massive MIMO Performance and Pilot Contamination

Youjia Chen, *Member, IEEE*, Ming Ding, *Senior Member, IEEE*, David López-Pérez, *Senior Member, IEEE*, Xuefeng Yao, Zihuai Lin, *Senior Member, IEEE*, and Guoqiang Mao, *Fellow, IEEE*

***Abstract*— In this paper, we theoretically analyse the uplink (UL) and downlink (DL) performance of massive multiple-input and multiple-output (mMIMO) networks, in term of coverage probability, cell spectral efficiency and network area spectral efficiency, using stochastic geometry. A sophisticated but yet practical system model is considered, taking into account a path loss model differentiating line-of-sight and non-line-of-sight transmissions, an idle mode capability at the base stations and a finite user density. Our analysis pays particular attention to the existence of a finite number of UL pilots for channel estimation and the effect of pilot contamination. We study for the first time the joint impact of the number of UL pilot sequences, the user density, and the base-station density on the pilot contamination issue in a mMIMO network, which in turn characterizes the DL and UL network performance. Moreover, using the proposed framework, we investigate two different scheduling problems—UE and pilot scheduling—, to find the optimal simultaneously scheduled UE density per time-frequency resource as well as the optimal UL pilot number to maximise the spectral efficiency.**

***Index Terms*— Massive MIMO, pilot contamination, coverage, spectral efficiency, stochastic geometry.**

I. Introduction

WIRELESS technologies are rapidly evolving to meet the performance demands of future applications, using 1) wider bandwidths to boost the amount of bits transmitted per unit of time, 2) more antennas to enhance the spectral efficiency, and thus the number of bits transmitted per unit of bandwidth, and 3) more cells to increase the spatial reuse, and thus the number of bits transmitted per unit of area.

Manuscript received May 30, 2020; revised November 19, 2020 and May 5, 2021; accepted July 23, 2021. Date of publication August 9, 2021; date of current version February 14, 2022. This work was supported by the National Nature Science Foundation of China under Grant 61801119. The associate editor coordinating the review of this article and approving it for publication was M. Guillaud. *(Corresponding author: Youjia Chen.)*

Youjia Chen is with Fujian Key Laboratory for Intelligent Processing and Wireless Transmission of Media Information, College of Physics and Information Engineering, Fuzhou University, Fuzhou 350108, China (e-mail: youjia.chen@fzu.edu.cn).

Ming Ding is with Data61, CSIRO, Sydney, NSW 2015, Australia (e-mail: ming.ding@data61.csiro.au).

David López-Pérez is with Huawei Technologies, 92100 Boulogne-Billancourt, France (e-mail: dr.david.lopez@ieee.org).

Xuefeng Yao is with Baidu Inc., Beijing 100085, China (e-mail: yaoxuefeng@baidu.com).

Zihuai Lin is with the School of Electrical and Information Engineering, The University of Sydney, Camperdown, NSW 2006, Australia (e-mail: zihuai.lin@sydney.edu.au).

Guoqiang Mao is with the Research Institute of Smart Transportation, Xidian University, Xi'an 710071, China (e-mail: g.mao@ieee.org).

Color versions of one or more figures in this article are available at https://doi.org/10.1109/TWC.2021.3101525.

Digital Object Identifier 10.1109/TWC.2021.3101525

Among the different features explored to implement such performance enhancement paradigms, the dense deployment of massive multiple-input and multiple-output (mMIMO) base stations (BSs) in urban areas is to attract much attention within both the academia and the industry. This is because dense mMIMO deployments can capture the benefits of both a larger number of BSs and a larger number of antennas per BS, i.e. spatial reuse and spatial multiplexing, respectively.

A. Background of mMIMO

mMIMO was invented at Bell Labs, and plainly speaking, refers to a technology feature where BSs are equipped with antenna arrays with many more antennas elements than user equipment (UE) to multiplex over the same time-frequency resource [1]. This large antenna array can excite a plurality of channel subspaces to support multiple simultaneous receptions from —or transmissions to— several UEs. In this way, the network capacity can potentially linearly grow with the number of spatial streams multiplexed. Due to the *channel hardening* effect, mMIMO is also more robust against the wireless channel fluctuations, which simplifies its operation [1].

Despite its significant benefits [2], mMIMO, also presents a number of challenges. Importantly, mMIMO requires channel state information (CSI) at the BS to realise the necessary multi-user uplink (UL) signal detection operations and downlink (DL) precoding ones. Most practical mMIMO implementations take advantage of the channel reciprocity of time division duplex (TDD) systems to acquire such CSI with the minimum possible overhead [3]. However, the number of orthogonal UL pilots in a given time-frequency resource is finite, which limits the number of UEs over which a BS can perform CSI acquisition at once. Hence, such UL pilots have to be reused across neighbouring BSs, and UEs allocated to the same UL pilot in neighbouring cells will interfere with each other in channel estimation phase, as shown in Fig. 1. This effect is known as *pilot contamination*, significantly affects the performance of mMIMO systems [4].

Pilot contamination has been identified as the main challenge to realise the theoretical mMIMO gains. In [1], the pioneering work of T. Marzetta showed *i)* how increasing the number of antennas leads to a larger network capacity and a smaller energy consumption, but also *ii)* that the CSI acquisition and the pilot contamination impose fundamental limits on what can be achieved with a noncooperative mMIMO system. Since then, a large body of research has touched upon the

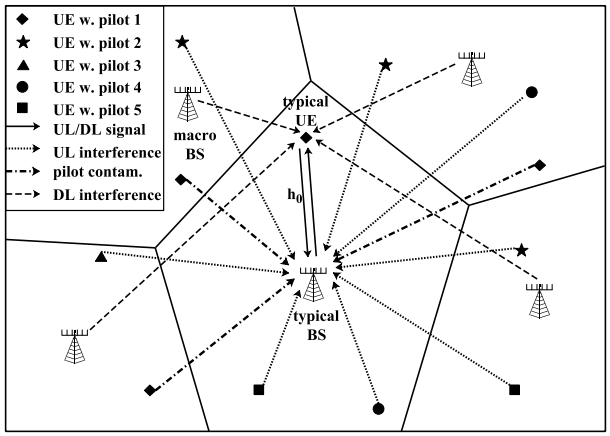

Fig. 1. An illustration of a mMIMO system with finite UE density considering pilot contamination.

pilot contamination problem, and proposed different methods to address the issue, from simpler UL pilot reuse schemes to more complex and sophisticated signal processing methods. For example, the performance of mMIMO systems under various linear receive filters and precoders, while considering pilot contamination, was analysed in [5]–[8]. All these theoretical works, however, are mostly based on a deterministic network topology, single cell or hexagonal multi-cell, and a given number of BSs and UEs, thus neglecting the randomness that governs practical networks.

To embrace more random deployments, stochastic geometry has been used to analyse network-wide mMIMO performance. In this area, the work of Bai and Heath [9] stands out, which investigated the UL mMIMO performance, while considering a mMIMO macrocell network and the pilot contamination. This paper presented a mMIMO capacity scaling law as a function of the number of antennas per BS and scheduled UEs, and analysed the performance gains attainable through a practical fractional UL pilot reuse. It is important to note, however, that this study assumed that there was a large number of UEs in each BS, and thus, that all BSs in the network were active and that all UL pilots available were in use in all BSs. Although reasonable for some macrocell scenarios, real-life traffic models indicate that many BSs may not be fully loaded, and only few active UEs are multiplexed together per TTI in MIMO systems, well below the capabilities of the BS [10]. Although reasonable for some macrocell scenarios, this consideration does not apply to all networks, particularly to denser ones, where some BSs may have no UEs in its coverage area or may not be fully loaded at a given point in time.

Similarly, in [11], Q. Zhang *et al.* studied the DL mMIMO performance, while considering a heterogeneous network comprised of mMIMO macrocells and single-antenna small cells, together with the effect of cross-tier interference. LoS and non-line-of-sight (NLoS) transmissions were embraced in this research, which have an important impact on performance. The asynchronous mode and the superimposed pilots in massive MIMO systems were analyzed in [12] and [13]. However, these works—similarly to the previous one—did not account for a realistic UE spatial distribution and a practical UL pilot-to-UE assignment either, which significantly affects the pilot contamination.

In [14], the massive MIMO system under a cell-free topology model is analysed, where an asymptotic analysis approach is adopted. The authors in [15] consider a fractional pilot reuse scheme for mMIMO by identifying the cell centre and cell edge areas, and investigate the UE distributions in them, where the pair correlation is considered due to the different pilot sets used in different zones.

B. Our Contributions

As depicted above, despite the number of papers the research is still quite scattered in this area and lacks generality. The main contributions of this paper are three-fold:

- We study both the UL and the DL performance of an mMIMO network with a realistic and sophisticated model, in which we consider finite BS and UE densities, a path loss function differentiating LoS and NLoS channels, an idle mode capability at BSs and a practical UL pilot-to-UE assignment.
- We theoretically analyse the pilot contamination in mMIMO networks by defining the point distributions of BSs and UEs reusing the same UL pilot, and quantify its impact on UL and DL SINRs.
- We investigate the performance impact of the scheduled UE density and the number of UL pilots, and show that there exists an optimal scheduled UE density and number of UL pilots to maximise the network capacity.

II. System Model

A. Network Scenario

We consider a TDD sub-6 GHz mMIMO cellular network consisted by macro-cell BSs as recommended by the 3GPP in [16]. As shown in Fig. 1, the distribution of the BSs follows a homogeneous Poisson point process (HPPP), $\Phi_b = \{\Phi \cup o\}$, where $\Phi \subset \mathcal{R}^2$, with a density of λ BSs/km^2, while the distribution of the active UEs accessing the network[1]—"UEs" for short— also follows another but independent HPPP, Φ_u, with a density of ρ UEs/km^2. Note that

- by the Slivnyak's theorem, the BS at the origin, o, becomes the typical BS, under the expectation over Φ_b,
- x_0 is the location of the typical UE served by the typical BS, and
- R_i denotes the distance between the i-th UE located at x_i and its serving BS located at y_i, while D_{ij} represents the distance between the i-th UE and an arbitrary non-serving BS located at y_j.

Each BS transmits with a constant power, P_d, and is equipped with M antennas. In the considered macro-cell scenario, the DL power is assumed to be equally allocated among the scheduled RBs [17], although it may lead to sub-optimal performance. While each UE is subject to UL

[1]Active UEs accessing the network are those that *i)* have been admitted into the network by the admission control procedure, and *ii)* have DL and/or UL data to transmit and/or receive. UEs with no data stay in idle mode, and are not considered in the analysis.

power control with a baseline power, P_u, and is equipped with only one antenna [18]. In more detail, we assume that fractional UL power control is in place, and thus, that the UL transmit power of a UE located at x_i can be defined as $P_i = P_u(\zeta_i)^{-\epsilon}$ where ζ_i is the path loss from such UE to its serving BS located at y_i, and $\epsilon \in [0,1]$ is the fraction of the path loss compensation.

With respect to the UL pilots, let us denote by $\mathbf{\Psi} = [\psi_1, \psi_2, \ldots, \psi_{K_\mathrm{T}}]$ the set of UL pilots available in the network, and thus in a BS, where $\mathbf{\Psi}^\mathrm{H}\mathbf{\Psi} = \tau\mathbf{I}$, and τ is the UL pilot sequence length. In order to design sequences with good orthogonality properties, we have $\tau \geq K_\mathrm{T}$.

B. Channel Model

We assume that the channel between any pair of transmit and receive antennas is i.i.d, and that consists of large-scale path loss and small-scale fading. Note that the channel is assumed quasi-static, that is, it stays constant within each frequency-time scheduling unit, but varies independently from one to another.

Regarding the large-scale path loss, we consider a practical model, which embraces LoS and NLoS transmissions. In more detail, denoting by r the distance between a pair of transmit and receive antennas, the path loss, $\zeta(r)$, between them can be formulated as

$$\zeta(r) = \begin{cases} \zeta^\mathrm{L}(r) = A^\mathrm{L} r^{-\alpha^\mathrm{L}}, & \mathrm{w.Pr}^\mathrm{L}(r), \\ \zeta^\mathrm{NL}(r) = A^\mathrm{NL} r^{-\alpha^\mathrm{NL}}, & \mathrm{w.Pr}^\mathrm{NL}(r), \end{cases} \tag{1}$$

where A^L and A^NL are the path losses at the reference distance $r = 1$ for the LoS and the NLoS cases, respectively, α^L and α^NL are the corresponding path loss exponents, and $\mathrm{Pr}_n^\mathrm{L}(r)$ and $\mathrm{Pr}_n^\mathrm{NL}(r)$ are the probabilities of having a LoS or a NLoS transmission, respectively, where $\int \left[\mathrm{Pr}_n^\mathrm{NL}(r) + \mathrm{Pr}_n^\mathrm{NL}(r)\right] \mathrm{d}r = 1$, and $\mathrm{Pr}_n^\mathrm{L}(r)$ monotonically decreases with the growth of r.

Regarding the small-scale fading, we consider a Rayleigh multi-path fading model[2], where $\mathbf{w} \in \mathcal{C}^{M\times 1}$ is the multi-path fading between the M antennas of a mMIMO array and its UE, with complex Gaussian distribution $\mathcal{CN}(\mathbf{0}, \mathbf{I}_M)$.

Based on the previous definitions, the channel gain, $\mathbf{h} \in \mathcal{C}^{M\times 1}$, can be expressed as $\mathbf{h} = \sqrt{\zeta(r)}\mathbf{w}$, where $\mathbf{h}_i = \sqrt{\zeta(R_i)}\mathbf{w}_i \triangleq \sqrt{\zeta_i}\mathbf{w}_i$ is the channel vector between the i-th UE located at x_i and its serving BS located at y_i, and $\mathbf{h}_{ij} = \sqrt{\zeta(D_{ij})}\mathbf{w}_{ij} \triangleq \sqrt{\zeta_{ij}}\mathbf{w}_{ij}$ is the interfering channel vector between such i-th UE and an arbitrary BS located at y_j.

C. UE Association Policy

In this paper, we consider a realistic user association process based on DL—and not on UL—measurements. In more detail, we adopt a practical criteria, where each UE is connected to the BS providing the maximum average received signal strength [21].

[2]In this work, we do not consider Rician fading for LoS transmissions and assume that there is a smart mMIMO scheduler, which schedules orthogonal UEs in each RB in each TTI [19], [20]. Involving Rician fading for LoS transmissions and Rayleigh fading for NLoS ones is one potential research direction for us in the future.

Considering the previous path loss model with LoS and NLoS transmissions, this UE association criteria, and denoting by R the random variable (RV) representing the distance between a UE and its serving BS, the LoS transmission PDF, $f_R^\mathrm{L}(r)$, and the NLoS transmission PDF, $f_R^\mathrm{NL}(r)$, at distance r, can calculated using the following expressions according [21],

$$f_R^\mathrm{L}(r) = \exp\left(-\int_0^{r_1} \mathrm{Pr}^\mathrm{NL}(u)\, 2\pi u\lambda \mathrm{d}u\right) \times \exp\left(-\int_0^{r} \mathrm{Pr}^\mathrm{L}(u)\, 2\pi u\lambda \mathrm{d}u\right) \mathrm{Pr}^\mathrm{L}(r)\, 2\pi r\lambda, \tag{2}$$

where $r_1 = \underset{r_1}{\arg}\left\{\zeta^\mathrm{NL}(r_1) = \zeta_n^\mathrm{L}(r)\right\}$, and

$$f_R^\mathrm{NL}(r) = \exp\left(-\int_0^{r_2} \mathrm{Pr}^\mathrm{L}(u)\, 2\pi u\lambda \mathrm{d}u\right) \times \exp\left(-\int_0^{r} \mathrm{Pr}^\mathrm{NL}(u) 2\pi u\lambda \mathrm{d}u\right) \mathrm{Pr}^\mathrm{NL}(r) 2\pi r\lambda, \tag{3}$$

where $r_2 = \underset{r_2}{\arg}\left\{\zeta^\mathrm{L}(r_2) = \zeta_n^\mathrm{NL}(r)\right\}$, respectively.[3]

III. On the Densities of BSs and UEs Reusing the Same UL Pilot

A. On the Density of Active BSs

In [22], the authors derived an approximate expression of the distribution of the Voronoi cell size, assuming that each UE is associated with the nearest BS. In [23], the authors proved that such approximated distribution still holds under the maximum average received signal strength association criteria, while embracing a path loss model with LoS and NLoS transmissions. However, the empirical value suggested for the Voronoi cell size has to be adjusted according to the specific path loss model.

Embracing this work, the authors in [24] showed that the number of UEs per BS, N_d, can be calculated using a Negative Binomial distribution, whose probability mass function (PMF) is given by

$$f_{N_d}(n) = \frac{\Gamma(n+Q)}{\Gamma(n+1)\Gamma(Q)} \left(\frac{\rho}{\rho+Q\lambda}\right)^n \left(\frac{Q\lambda}{\rho+Q\lambda}\right)^Q, \tag{4}$$

where $\Gamma(\cdot)$ is the Gamma function, an Q is the fitting parameter used to adjust the Voronoi cell size to the specific path loss model.

Since a BS may have no UE associated to it, i.e $N_d = 0$, and because such BS would enter in idle mode —mute its transmissions— to mitigate interference and save energy [23], [25], the set of active BSs that generate interference is defined as follows:

Definition of Active BSs: Denoting by $\tilde{\Phi}_b$ the set of active BSs —those that have at least one UE connected to it—, $\tilde{\Phi}_b$

[3]Note that, in some existing works the authors consider a different user deployment, e.g. one UE per Voronoi cell, which makes the BS and UE distributions intertwined and leads to a different PDF of link distance. In contrast, we assume that the UE distribution is independent with the BS one.

TABLE I
SUMMARY OF NOTATIONS

Notation	Description
Φ_b, $\tilde{\Phi}_b$, $\tilde{\Phi}_b^{(k)}$; λ, $\tilde{\lambda}$, λ_k	set of BSs, active BSs, and active BSs allocating the k-th pilot; the corresponding densities of above point processes
Φ_u $\tilde{\Phi}_u$, $\tilde{\Phi}_u^{(k)}\backslash x_0$; ρ, $\tilde{\rho}$, $\rho_k(x)$	set of UEs, simultaneously transmitting UEs, interfering UEs allocating the k-th pilot; the corresponding densities of above point processes
P_d, P_u, P_i	DL transmit power, baseline UL power, UL transmit power of a UE located at x_i
N_d, N, $\bar{N}$	the number of UEs and simultaneously transmitting UEs in a cell, the expected number of N
M, K_{T}, τ	the number of antennas and pilot numbers, the length of pilot sequence
$\mathbf{\Psi}$, ψ_k	set of UL pilots, the k-th pilot
ζ_i, $\mathbf{w}_i$, $\mathbf{h}_i$ ζ_{i0}, $\mathbf{w}_{i0}$, $\mathbf{h}_{i0}$	the path loss, multi-path fading and channel vectors between UE x_i and its serving BS y_i the path loss, multi-path fading and channel vectors between UE x_i and the typical BS
$\bar{\mathbf{h}}_0$, $\hat{\mathbf{e}}_0$ $\mathbf{g}_0^*$, $\mathbf{u}_0$	estimated channel and channel estimation error of the typical UE the UL combining vector and DL precoding vector of typical UE
$\mathrm{SINR_U}(r)$, $\mathrm{SINR_D}(r)$	the UL and DL SINR with the serving distance r

can be approximated by a thinned HPPP with density [26]

$$\tilde{\lambda} = \lambda \cdot \left(1 - \left(\frac{Q\lambda}{\rho + Q\lambda}\right)^{Q}\right). \tag{5}$$

B. On the Density of Simultaneously Transmitting UEs

In modern TDD systems, CSI acquisition is driven by UL pilots. Unfortunately, the number of existing orthogonal UL pilots that can be generated in a given time-frequency resource is finite, and mostly defined by the system bandwidth and numerology. This limits the number of UEs over which a BS can perform CSI acquisition at once.

Assuming that the number of UL pilots available for CSI acquisition in the network is K_{T}, and that the CSI of every UE has to be acquired prior to every transmission, a BS can at most serve K_{T} UEs in a given time-frequency scheduling unit. Considering this constraint, we can derive the number of simultaneously transmitting UEs in a BS, N, as $N = \min(N_d, K_{\mathrm{T}})$, whose PMF can be calculated as

$$f_N(n) = \begin{cases} \dfrac{f_{N_d}(n)}{1 - f_{N_d}(0)}, & 1 \le n \le K_{\mathrm{T}} - 1 \\ \dfrac{\sum_{n=K_{\mathrm{T}}}^{+\infty} f_{N_d}(n)}{1 - f_{N_d}(0)} & n = K_{\mathrm{T}}, \end{cases} \tag{6}$$

where $1 - f_{N_d}(0)$ is the probability of a BS being active with at least one transmitting UE, and $\sum_{n=K_{\mathrm{T}}}^{+\infty} f_{N_d}(k)$ is the probability of a BS being fully loaded with K_{T} simultaneously transmitting UEs. With this, we can compute the expected number of simultaneously transmitting UEs in an active BS, $\bar{N}$, as $\bar{N} = \sum_{n=1}^{K_{\mathrm{T}}} n \cdot f_N(n)$ and make the following definition:

Definition of Simultaneously Transmitting UEs: Denoting by $\tilde{\Phi}_u$ the set of simultaneously transmitting UEs in the network, $\tilde{\Phi}_u$ can be approximated by an HPPP with density

$$\tilde{\rho} = \tilde{\lambda}\bar{N}. \tag{7}$$

The approximation used here is based on the fact that there are multiple UEs simultaneously transmitting in each cell of the mMIMO system. With respect to the typical BS located at the origin, the spatial correlation is weak since the pilot number is always large.

From the above derivations, we draw the following remarks.

Remark 1: For a given λ, both $\bar{N}$ and $\tilde{\rho}$ increase with the increase of ρ.

Remark 2: For a given λ and a given ρ, both $\bar{N}$ and $\tilde{\rho}$ increase with the increase of K_{T}.

Remark 3: $\tilde{\rho}$ is upper bounded by $\min\{\rho, \tilde{\lambda}K_{\mathrm{T}}\}$.

C. On the Densities of BSs and UEs Reusing an UL Pilot

If the number of simultaneously transmitting UEs in a BS, N, is less than the number of UL pilots available for CSI acquisition in the network, K_{T}, i.e. $N < K_{\mathrm{T}}$, then not all the UL pilots available are in use in such BS. This leads to a reduced probability of UL pilot collision in neighbouring cells, and thus to a reduced pilot contamination. Given the number of simultaneously transmitting UEs in a BS, N, and assuming that the UL pilots are randomly and uniformly allocated to UEs in every BS, the probability of a random UL pilot being used in a BS is $\frac{N}{K_{\mathrm{T}}}$.

Considering the PMF, $f_N(n)$, of such number of simultaneously transmitting UEs in a BS, N, we can further derive the average probability of an UL pilot being used in the network as $\sum_{n=1}^{K_{\mathrm{T}}} \frac{n}{K_{\mathrm{T}}} \cdot f_N(n)$, and make other two definitions and remarks that are useful to quantify the effect of pilot contamination.

Definition of Active BSs Allocating the k-th UL Pilot: Denoting by $\tilde{\Phi}_b^{(k)}$ the set of active BSs allocating the k-th UL pilot, $\forall k \in [1, \ldots, K_{\mathrm{T}}]$, $\tilde{\Phi}_b^{(k)}$ can be approximated by a thinned HPPP with density

$$\lambda_k = \tilde{\lambda}\frac{\sum_{n=1}^{K_{\mathrm{T}}} n \cdot f_N(n)}{K_{\mathrm{T}}} = \tilde{\lambda}\frac{\bar{N}}{K_{\mathrm{T}}} = \frac{\tilde{\rho}}{K_{\mathrm{T}}}. \tag{8}$$

Definition of Interfering UEs Allocated With the k-th UL Pilot: Denoting by $\tilde{\Phi}_u^{(k)}\backslash x_0$ the set of interfering UEs allocated with the k-th UL pilot, $\forall k \in [1, \ldots, K_{\mathrm{T}}]$, assuming the typical UE is allocated with such k-th UL pilot, $\tilde{\Phi}_u^{(k)}\backslash x_0$ can be defined as a non-stationary point process due to the BS-UE pair correlations. Although the exact distribution of such non-stationary point process is hard to derive, according to [27], it can be well approximated by an HPPP with density

$$\rho_k(x) = \lambda_k \left(1 - \exp\left(-\frac{12}{5}\lambda_k \pi x^2\right)\right), \tag{9}$$

where x is the distance between an interfering UE in another cell and the typical BS.

Remark 4: For a given a K_{T}, λ_k increases with the increase of λ and ρ.

Remark 5: For a given λ and a given ρ, λ_k monotonically decreases with the increase of K_{T}.

IV. Analysis on UL and DL SINRs

A. On the Channel Estimation With Pilot Contamination

UEs allocated with the same UL pilot in neighbouring cells will interfere with each other in the channel estimation phase, which in turn affects the quality of the UL receive filter and/or DL precoder. Without loss of generality, assume that the typical UE is allocated to the first UL pilot, under the assumption of a synchronised network. As a result, the received UL pilot signal at the typical BS, located at the origin, o, can be expressed as $\mathbf{Y}_o = \sum_{k=1}^{K_T} \sum_{x_i \in \tilde{\Phi}_u^{(k)}} \sqrt{P_i}\mathbf{h}_{i0}\psi_k^{\mathrm{T}} + \mathbf{N}_u$, where $\mathbf{N}_u \in \mathcal{C}^{M\times\tau}$ is an UL additive white Gaussian noise (AWGN) matrix, whose elements are i.i.d with zero mean and variance σ^2. That is, theoretically, the typical BS receives the UL pilot signals sent from all UEs simultaneously transmitting in the network.

To estimate the UL channel of the typical UE, $\bar{\mathbf{h}}_0$, the typical BS will project the received UL pilot signal, $\mathbf{Y}_o$, onto the conjugate of the first pilot, ψ_1^*. When a minimum mean square error (MMSE) estimator is considered, the estimate of the UL channel of the typical UE, $\bar{\mathbf{h}}_0$, can be calculated as $\bar{\mathbf{h}}_0 = \eta_0 \mathbf{Y}_0 \psi_1^* = \eta_o \left(\sum_{x_i \in \tilde{\Phi}_u^{(1)}} \sqrt{P_i}\mathbf{h}_{i0} + \mathbf{N}_u \psi_1^* \right)$, where the coefficient $\eta_0 = \frac{\sqrt{P_0}\zeta_0}{\sum_{x_i \in \tilde{\Phi}_u^{(1)}} P_i \zeta_{i0} + \frac{\sigma^2}{\tau}}$. Hence, the estimation error follows a Gaussian distribution, i.e., $\hat{\mathbf{e}}_0 \sim \mathcal{CN}\left(\mathbf{0}, \zeta_0 \left(1 - \frac{P_0\zeta_0}{P_0\zeta_0 + \sum\limits_{x_i \in \tilde{\Phi}_u^{(1)}/0} P_i\zeta_{i0} + \frac{\sigma^2}{\tau}}\right)\mathbf{I}_M\right)$.

From the above formulation, we can see that the estimation error for the typical UE originates from *i)* the noise in the UL channel—with power σ^2—, and *ii)* the interference caused by UEs in other cells scheduled with the same UL pilot, i.e. the pilot contamination. Obviously, this shows that the density of the point process, $\tilde{\Phi}_u^{(k)}$, i.e. λ_k, is the key factor of the magnitude of the pilot contamination.

B. Analysis on the UL SINR

With respect to the received UL data, a BS will use its UL channel estimates to detect the UL data sent by its UEs. Assuming maximum ratio combining (MRC) at the receiver, which maximises the received SNR, we have that the combining vector to receive the data from the typical UE can be expressed as $\mathbf{g}_0^* = \frac{1}{\eta_0}\bar{\mathbf{h}}_0$. Denoting by v_i the UL data symbol sent from UE x_i, the decoded symbol for the typical UE can be formulated as $\hat{v}_0 = \mathbf{g}_0^{\mathrm{T}}\left(\sum_{x_i \in \tilde{\Phi}_u} \sqrt{P_i}\mathbf{h}_{i0}v_i + \mathbf{n}_u\right)$, and the UL SINR for the typical UE received at the typical BS can be expressed as

$$\mathrm{SINR_U} = \frac{P_0|\mathbf{g}_0^{\mathrm{H}}\bar{\mathbf{h}}_0|^2}{P_0\mathbb{E}_{\hat{\mathbf{e}}_0}\left[|\mathbf{g}_0^{\mathrm{H}}\hat{\mathbf{e}}_0|^2\right] + \sum\limits_{x_i \in \tilde{\Phi}_u \setminus x_0} P_i \mathbb{E}_{\mathbf{w}_{i0}}\left[|\mathbf{g}_0^{\mathrm{H}}\mathbf{h}_{i0}|^2\right] + |\mathbf{g}_0^{\mathrm{H}}|^2\sigma^2}, \tag{10}$$

where the expectations are taken over the channel estimation error, $\hat{\mathbf{e}}_0$, and the small-scale fading, $\mathbf{w}_{i0}$, in the interference links' channel gains, $\mathbf{h}_{i0}$, as in Eq. (8) in [9]. This SINR expression is still a random variable, due to the randomness in the large scale path losses.

Theorem 1: Given the serving distance r, the UL SINR can be calculated as

$$\begin{aligned}\mathrm{SINR_U}(r) &= P_u(M+1)\zeta(r)^{2(1-\epsilon)} \Big/ \Big(\zeta(r)^{1-\epsilon}\Big(P_u\mathrm{A}(\lambda_1) + \frac{\sigma^2}{\tau}\Big) \\ &\quad + MP_u\mathrm{A}^2(\lambda_1) + \big(P_u\mathrm{B}(\tilde{\rho}) + \sigma^2\big) \\ &\quad \times \Big(\zeta(r)^{1-\epsilon} + \mathrm{A}(\lambda_1) + \frac{\sigma^2}{P_u\tau}\Big)\Big). \end{aligned} \tag{11}$$

In the equation, the pilot contamination-related function $\mathrm{A}^a(\lambda_1)$ is used to calculate $\mathbb{E}\left[\sum_{x_i \in \tilde{\Phi}_u^{(k)} \setminus x_0} \left(\zeta_{i0}\left(\zeta_i\right)^{-\epsilon}\right)^a\right]$, whose formulation is presented in (26), and the UL data interference-related function $\mathrm{B}(\tilde{\rho})$ is used to calculate $\mathbb{E}\left[\sum_{x_i \in \tilde{\Phi}_u \setminus x_0} \zeta_{i0}\left(\zeta_i\right)^{-\epsilon}\right]$, whose detail formulation is presented in (27).

Proof: See Appendix A.

Considering the UL signal may be in either LoS or NLoS, substituting $\zeta(r) = \zeta^{\mathrm{L}}(r)$ for an LoS signal or $\zeta(r) = \zeta^{\mathrm{NL}}(r)$ for an NLoS signal in Eq. (11), we can obtained the corresponding SINR, $\mathrm{SINR_U^L}(r)$ and $\mathrm{SINR_U^{NL}}(r)$.

1) Impact of the Pilot Contamination: From Appendix A, we can re-formulate the received UL interference, $\mathrm{I_U^{agg}}|_{\sigma^2=0}$, as follows—where the noise is neglected for a clearer formulation—,

$$\begin{aligned}\mathrm{I_U^{agg}}|_{\sigma^2=0} &= MP_u^2\zeta(r)^{1-\epsilon}\Big(\mathrm{A}(\lambda_1) + \mathrm{B}(\tilde{\rho})\Big) \\ &\quad + MP_u^2\mathrm{B}(\tilde{\rho})\mathrm{A}(\lambda_1) + M^2P_u^2\mathrm{A}^2(\lambda_1). \end{aligned} \tag{12}$$

From this formulation, we can clearly see that the pilot contamination, represented by $\mathrm{A}(\lambda_1)$, impacts all components of the received UL interference, $\mathrm{I_U^{agg}}|_{\sigma^2=0}$. With this in mind, we were able to define the received UL interference due to the pilot contamination, $\mathrm{I_U^{PC}}$, as follows

$$\mathrm{I_U^{PC}}|_{\sigma^2=0} = MP_u^2\Big(\zeta(r)^{1-\epsilon} + \mathrm{B}(\tilde{\rho})\Big)\mathrm{A}(\lambda_1) + M^2P_u^2\mathrm{A}^2(\lambda_1), \tag{13}$$

and show that the pilot contamination-related function, $\mathrm{A}(\lambda_1)$, works as a multiplier in $\mathrm{I_U^{PC}}|_{\sigma^2=0}$. From the formulation of (26), the pilot contamination-related function, $\mathrm{A}^a(\lambda_k)$, increases monotonically with the density, λ_k, and approaches its limit when $\lambda_k \to \lambda$. Hence, the received UL interference will also increase with λ_k.

2) Impact of λ, ρ and K_{T}: From (8), i.e. $\tilde{\rho} = K_{\mathrm{T}}\lambda_k$, we can see that both the density of simultaneously transmitting UEs in the network, $\tilde{\rho}$, and the density of BSs reusing the a UL pilot, λ_1, are intimately related, and that they depend on the BS density, λ, and the UE density, ρ. Based on the result in this section, we have the following remarks:

Remark 6: For a given λ and a given K_{T}, $\mathrm{A}(\lambda_1)$ and $\mathrm{B}(\tilde{\rho})$ increase with the increase of ρ according to *Remark 1* and *Remark 4*, which contributes to the growth of the aggregated interference, $\mathrm{I_U^{agg}}|_{\sigma^2=0}$.

Remark 7: For a given λ and a given ρ, the increase of K_{T} has two contradicting impacts on $\mathrm{I}_{\mathrm{U}}^{\mathrm{agg}}|_{\sigma^2=0}$:

- The larger K_{T}, the larger $\tilde{\rho}$, which in turn also increases $\mathrm{B}(\tilde{\rho})$ and hence increases the interference. However, note that this increase stops when the number of interfering sources reaches its maximum, i.e. when $\tilde{\rho} \to \rho$.
- The larger K_{T}, the smaller λ_1, which in turn also decreases $\mathrm{A}(\lambda_1)$ and hence relieves the interference.

Remark 8: For a given ρ and a given K_{T}, λ shows a trade-off on $\mathrm{SINR}_{\mathrm{U}}$:

- The signal increases with the increase of λ due to a shorten signal distance.
- $\mathrm{I}_{\mathrm{U}}^{\mathrm{agg}}|_{\sigma^2=0}$ also increases with the increase of λ, as both $\tilde{\rho}$ and λ_1 increase with the increase of λ. However, note that the increase of $\mathrm{I}_{\mathrm{U}}^{\mathrm{agg}}|_{\sigma^2=0}$ stops when $\tilde{\rho} \to \rho$.

C. Analysis on the DL SINR

With respect to the transmit DL data, a BS will use its UL channel estimates to precode the DL data. Assuming maximum ratio transmission (MRT) at the transmitter, which also maximises the received SNR, we have that the precoding vector to transmit the data to the typical UE can be expressed as $\mathbf{u}_0 = \kappa_0 \bar{\mathbf{h}}_0$, where $\kappa_0 = \frac{1}{\sqrt{N_0 \cdot |\bar{\mathbf{h}}_0|^2}}$, if the DL transmit power is equally allocated to all such UEs, and N_0 is the number of UEs simultaneously receiving data in the typical BS. Denoting by v_0 the DL data symbol sent to UE x_i, the received symbol at the typical UE can be formulated as $\check{v}_0 = \sum_{y_j \in \tilde{\Phi}_b} \mathbf{h}_{0j}^{\mathrm{H}} \sum_{x_i \in \mathcal{V}(y_j)} \sqrt{P_d}\mathbf{u}_i v_i + \mathbf{n}_d$, where $\mathbf{n}_d \in \mathcal{C}^{M\times 1}$ is an DL AWGN vector, whose elements are i.i.d with zero mean and variance σ^2, and the DL SINR received at the typical UE can be expressed as

$$\mathrm{SINR}_{\mathrm{D}} = \frac{P_d |\bar{\mathbf{h}}_0^{\mathrm{H}} \mathbf{u}_0|^2}{P_d \mathbb{E}_{\hat{\mathbf{e}}_0}\left[|\hat{\mathbf{e}}_0^{\mathrm{H}} \mathbf{u}_0|^2\right] + \sum\limits_{\substack{y_j \in \tilde{\Phi}_b, \\ x_i \in V(y_j) \\ i \neq 0}} P_d \mathbb{E}_{\mathbf{w}_{i0}}\left[|\mathbf{h}_{0j}^{\mathrm{H}} \mathbf{u}_i|^2\right] + \sigma^2}, \tag{14}$$

where similar to the UL SINR the expectation operators are taken over the channel estimation error $\hat{\mathbf{e}}_0$ and small-scale fading $\mathbf{w}_{i0}$ in the interference links' channel gain $\mathbf{h}_{i0}$.

Theorem 2: Given the serving distance r, the DL SINR can be calculated as

$$\begin{aligned}\mathrm{SINR}_{\mathrm{D}}(r) &= (M+1)\zeta(r)^{2-\epsilon} \Big/ \Bigg(\Big(\zeta(r) + \frac{\sigma^2 \bar{N}}{M P_d}\Big)\Big(\mathrm{A}(\lambda_1) + \frac{\sigma^2}{P_u \tau}\Big) \\ &\quad + M\mathrm{C}^2(\lambda_1)\zeta(r)^{-\epsilon} + \mathrm{C}(\tilde{\lambda})\Big(\frac{\sigma^2}{P_u \tau} + \mathrm{B}(\tilde{\rho})\Big)\Bigg). \end{aligned} \tag{15}$$

In the above formulation, the DL interferers-related function, $\mathrm{C}^a(b)$, is used to calculate the term, $\mathbb{E}\left[\sum\limits_{y_j \in \tilde{\Phi}_b \setminus y_0} (\zeta_{0j})^a\right]$ and the term, $\mathbb{E}\left[\sum\limits_{y_j \in \tilde{\Phi}_b^{(1)} \setminus y_0} (\zeta_{0j})^2\right]$, involved in the calculation of the second item in denominator of SINR, whose formulation is presented in (28) and b denotes the density of related HPPP.

Proof: See Appendix B.

1) Impact of the Pilot Contamination and Densities: Similar to the UL SINR, the impact of the pilot contamination exists in the interference part. It lies on the auxiliary functions $\mathrm{A}(\cdot)$ and $\mathrm{C}(\cdot)$ with parameter λ_1, which represents the density of BSs reusing the first UL pilot, and plays a role in all the three components of the received DL interference. Importantly, the misalignment of all the precoder vectors of all scheduled UEs in the system due to the pilot contamination makes the impact of the pilot contamination more complicated to isolate in the DL SINR than in the UL one.

Based on the result in this section, we have the following remarks:

Remark 9: For a given λ and K_{T}, the aggregated interference, $\mathrm{I}_{\mathrm{D}}^{\mathrm{agg}}$, increases with the increase of ρ. This is due to the larger λ_1—and the resulting severer pilot contamination—, the larger $\tilde{\rho}$ and the larger $\tilde{\lambda}$.

Remark 10: Similar to $\mathrm{SINR}_{\mathrm{U}}$, for a given ρ and a given K_{T}, the BS density λ also shows a trade-off on $\mathrm{SINR}_{\mathrm{D}}$:

- The signal increases with the increase of λ.
- The aggregated interference $\mathrm{I}_{\mathrm{D}}^{\mathrm{agg}}$ also increases with λ, as both $\tilde{\rho}$ and $\tilde{\lambda}$ increase with the growth of λ. However, note that the increase of $\mathrm{I}_{\mathrm{D}}^{\mathrm{agg}}$ stops when $\tilde{\rho} \to \rho$. While the signal still continues to grow with λ.

V. Performance Metrics and Optimal Scheduling Problems

A. SINR Distribution and Coverage Probability

According to [9], the CCDFs of the received UL and the received DL SINRs—when considering LoS and NLoS—can be computed by

$$\begin{aligned}\Pr\left[\mathrm{SINR} > \delta\right] = \int_0^{+\infty} &\Pr\left[\mathrm{SINR}^{\mathrm{L}}(r) > \delta\right] f_R^{\mathrm{L}}(r) \\ &+ \Pr\left[\mathrm{SINR}^{\mathrm{NL}}(r) > \delta\right] f_R^{\mathrm{NL}}(r) \mathrm{d}r. \end{aligned} \tag{16}$$

Given a SINR threshold γ, the UL and DL coverage probabilities can be defined as the probabilities that the received UL and DL SINRs are larger than such SINR threshold, i.e.

$$p^{\mathrm{cov}}(\lambda, \rho, K_{\mathrm{T}}, \gamma) \triangleq \Pr\left[\mathrm{SINR} > \gamma\right]. \tag{17}$$

From this CCDF formulations of the received UL and the received DL SINRs, the UL and the DL coverage probabilities can be easily obtained using such CCDFs and the SINR threshold.

Corollary 1: Given the BS density, λ, both the UL and the DL coverage probabilities, p^{cov}, decrease with the UE density, ρ.

B. Per-BS Spectral Efficiency and Area Spectral Efficiency

Considering the average number of simultaneously transmitting UEs in a BS, $\bar{N}$, the sum spectral efficiency in the typical BS can be derived as

$$\begin{aligned}&\mathrm{S}(\lambda, \rho, K_{\mathrm{T}}, \gamma_0) \\ &= \Big(1 - \frac{\eta}{T}\Big) \sum_{n=1}^{K_{\mathrm{T}}} n f_N(n) \int_{\gamma_0}^{+\infty} \log_2(1+\gamma) f_{\Gamma}(\lambda, \rho, K_{\mathrm{T}}, \gamma) d\gamma \\ &= \Big(1 - \frac{\eta}{T}\Big) \frac{\bar{N}}{\ln 2} \int_{\gamma_0}^{+\infty} \frac{p^{\mathrm{cov}}(\lambda, \rho, K_{\mathrm{T}}, \gamma)}{1+\gamma} d\gamma \\ &\quad + \Big(1 - \frac{\eta}{T}\Big) \bar{N} \log_2(1+\gamma_0) \cdot p^{\mathrm{cov}}(\lambda, \rho, K_{\mathrm{T}}, \gamma_0), \end{aligned} \tag{18}$$

where $f_\Gamma(\lambda, \rho, K_\mathrm{T}, \gamma)$ is the PDF of the received SINR, and η is the number of OFDM symbols dedicated to the transmission of UL pilots within the T OFDM symbols of a subframe. Since only $T - \eta$ OFDM symbols are allocated to user data, either UL or DL, $\frac{\eta}{T}$ represents the fraction of pilot overhead. Note that the overhead, η, is a function of both the length of the UL pilot sequence, τ, and the number of such UL pilots, K_T. Fixing the length of the UL pilot sequence, τ, the overhead, η, can be formulated as a linear function of K_T.

To represent the entire network performance, we use the ASE in bps/Hz/km^2, which was defined in [28], and can be calculated as

$$\mathrm{ASE} = \tilde{\lambda} \cdot \mathrm{S}(\lambda, \rho, \mathrm{K_T}, \gamma_0). \tag{19}$$

C. UE Scheduling Problem

From *Remark 6,* one can conclude that for any typical UE, its UL SINR, $\mathrm{SINR_U}$, decreases with the UE density, ρ. However, from *Remark 1*, $\bar{N}$ in the formulation of per-BS spectral efficiency increases with it. Inspired by this trade-off, the performance impact of the UE density, ρ, is further investigated here.

Lemma 1: The density of simultaneously transmitting UEs in the network, $\tilde{\rho}$, is a concave (downward) function with the increase of the UE density, ρ.

Proof: See Appendix C.

Lemma 2: If we do not consider the pilot contamination, i.e. $\lambda_k = 0$, and neglect the UL noise power, $\sigma^2 = 0$, the ASE is a concave (downward) and monotonically increasing function with the increase of the UE density, ρ, and approaches its limit when $\lim_{\rho \to \infty} \tilde{\rho} = K_\mathrm{T}\lambda$.

Proof: See Appendix D.

Theorem 3: If we consider the pilot contamination, the ASE is not monotonically increasing with the increase of the UE density, ρ.

Proof: See Appendix E.

Intuitively, the pilot contamination increases the received UL interference power, and breaks the monotonically increasing law of the ASE in Lemma 2. The more UEs, the severer the pilot contamination, and thus the more chances that the ASE is not a monotonically increasing function.

Based on this analysis, we can conclude that there may be an optimal density of UEs admitted to access the network, ρ^*, in the presence of pilot contamination to maximise the ASE, $\mathrm{ASE}\,(\lambda, \rho, K_\mathrm{T}, \gamma_0)$. Thus, we propose the following **UL UE scheduling problem**: *"For a given BS density, λ, and number of UL pilots available in the network, K_T, which is the optimal density of UEs admitted to access the network, ρ^*, that can maximise the ASE?"*. That is,

$$\begin{aligned} &\underset{\rho}{\text{maximize}}\ \mathrm{ASE}\,(\lambda, \rho, K_\mathrm{T}, \gamma_0) \\ &\text{s.t. } 0 < \rho \leq \rho_0, \end{aligned} \tag{20}$$

where ρ_0 denotes the overall UE density—with and without network access—, and the constraint guarantees the density of UEs admitted to access the network is less than ρ_0.

Due to the complexity of the formulations of the SINR, it is very difficult to directly find the optimal density of UEs admitted to access the network, ρ^*, and we take this challenge for our future work. However, from the derivation process of the above theorem, we can make following important remark:

Remark 11: Admitting all UEs to simultaneously access the network is not always the best strategy to maximise the ASE, the optimal density of UEs admitted to access the network, ρ^*, highly depends on the BS density, λ, and the number of UL pilots available in the network, K_T.

D. Pilot Scheduling Problem

The network performance also shows a complex behaviour with the number of UL pilots available in the network, K_T. We should highlight that:

- The efficiency factor $(1 - \frac{\eta}{T})$ in (18) monotonically decreases with the increase of the number of UL pilots available in the network, K_T.
- The received UL signal power is independent of K_T.
- The received UL interference, $\mathrm{I_U^{agg}}$, presents a trade-off with the increase of K_T according to *Remark 7*, i.e. the larger K_T, the more simultaneously transmitting UEs, and thus the more interfering sources. However, once all UEs are transmitting, the larger K_T, the less pilot contamination.
- The average number of simultaneously transmitting UE, $\bar{N}$, increases with the increase of K_T as indicated in *Remark 2*. As a result, the spatial reuse and multiplexing increase too, until all UEs are transmitting.

To better focus on the impact of the number of UL pilots available in the network, K_T, let us consider the following scenario where the UE density, ρ, is large enough compared to the BS density, λ, i.e. $\rho \gg \tau\lambda$, and have the following theorem.

Theorem 4: The sum spectral efficiency, S, is a concave function with the increase of the number of UL pilots, K_T, thus there exists an optimal K_T to maximise it.

Proof: See Appendix F.

Based on the above analysis, the following **UL pilot scheduling problem** arises: *"In a heavy-load network, what is the optimal number of UL pilots available in the network, K_T^*, that can maximise the sum spectral efficiency in the typical BS?"*. That is,

$$\begin{aligned} &\max_{K_\mathrm{T}}\ \mathrm{S}(\lambda, \rho, K_\mathrm{T}, \gamma_0) \\ &s.t.\ 1 \leq K_\mathrm{T} \leq \min\{M, \tau\}. \end{aligned} \tag{21}$$

where the constraint guarantees that the number of UL pilots available in the network, K_T, is smaller than the number of antennas, M, and can be accommodated in η OFDM symbols.

To find the optimal number of UL pilots available in the network, K_T^*, Algorithm 1 is proposed. Note that this algorithm can also work in a light-loaded network, where all UL pilots do not need to be in use.

VI. Results and Discussions

Embracing practical simulation assumptions in this study, the 3GPP model and parameters listed in Tables A.1-3 and A.1-7 of [29] are adopted. That is: $M = 64$, $\epsilon = 0.8$,

Algorithm 1 The Proposed Algorithm to Find K_{T}^{*}

Step 1: Initialization

- Set $K_{\mathrm{T}}^{\mathrm{left}}=0$, $K_{\mathrm{T}}^{\mathrm{right}}=\min M,\tau$;

Step 2: Iteration

- Compute $K_{\mathrm{T}}^{\mathrm{lm}}=K_{\mathrm{T}}^{\mathrm{left}}+\frac{K_{\mathrm{T}}^{\mathrm{right}}-K_{\mathrm{T}}^{\mathrm{left}}}{3}$, $K_{\mathrm{T}}^{\mathrm{rm}}=K_{\mathrm{T}}^{\mathrm{right}}-\frac{K_{\mathrm{T}}^{\mathrm{right}}-K_{\mathrm{T}}^{\mathrm{left}}}{3}$; and $\mathrm{S}^{\mathrm{lm}}\left(\lambda,\rho,K_{\mathrm{T}}^{\mathrm{lm}},\gamma_0\right)$, $\mathrm{S}^{\mathrm{rm}}\left(\lambda,\rho,K_{\mathrm{T}}^{\mathrm{rm}},\gamma_0\right)$ using (18).
- If $\mathrm{S}^{\mathrm{lm}}<\mathrm{S}^{\mathrm{rm}}$, update $K_{\mathrm{T}}^{\mathrm{left}}=K_{\mathrm{T}}^{\mathrm{lm}}$;
  Else, update $K_{\mathrm{T}}^{\mathrm{right}}=K_{\mathrm{T}}^{\mathrm{rm}}$.

Step 3: Termination

- If $K_{\mathrm{T}}^{\mathrm{right}}-K_{\mathrm{T}}^{\mathrm{left}}<\epsilon$, terminate.
  Else, go to Step 2.

Step 4: Output

- $K_{\mathrm{T}}^{*}=\frac{K_{\mathrm{T}}^{\mathrm{left}}+K_{\mathrm{T}}^{\mathrm{right}}}{2}$.

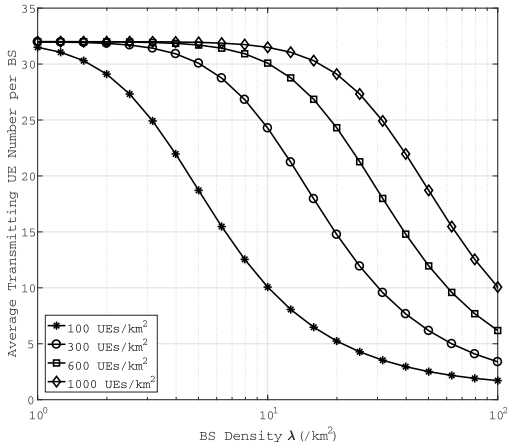

Fig. 2. Average simultaneously transmitting UE number per BS, $\bar{N}$, vs. the BS density, λ, with different UE density, ρ.

$K_{\mathrm{T}}=32$, $\tau=K_{\mathrm{T}}$, $\alpha^{\mathrm{L}}=2.09$, $\alpha^{\mathrm{NL}}=3.75$, $A^{\mathrm{L}}=10^{-10.38}$, $A^{\mathrm{NL}}=10^{-14.54}$, $P_u=24$dBm and $P_d=46$dBm. Moreover, according to LTE specifications and with regard to overhead, $\eta=1$, 3 and 4 for $K_{\mathrm{T}}=16$, 48 and 64, respectively. The SINR threshold is set to $\gamma_0=0$dB. In the simulations, the instantaneous signal and aggregated interference are calculated for 1000 spatial realizations to obtain the average coverage probability and spectral efficiency.

In Fig. 2, we plot the average number of simultaneously transmitting UEs in a BS, $\bar{N}$, with respect to the BS density, λ, for various UE densities, ρ. From this figure, we can observe that 1) $\bar{N}$ decreases with the increase of λ or the decrease of ρ; 2) $\bar{N}$ is upper bounded by K_{T}; 3) Such upper bound—maximum load—is reached in deployments with small λ and large ρ, i.e. under dimensioned networks.

Moreover, in Fig. 3 we plot the density of scheduled UEs using the same pilot, λ_k, with respect to the BS density, λ, for various UE densities, ρ. From the figure, we can see that 1) λ_k increases with the increase of λ and ρ, and has the limit, $\frac{\rho}{K_{\mathrm{T}}}$. This observation is in line with Remark 4. 2) When the BS density is very small, i.e. $\lambda\ll\rho$, the UL pilots are fully reused in each BS, and thus $\lambda_k\approx\lambda$.

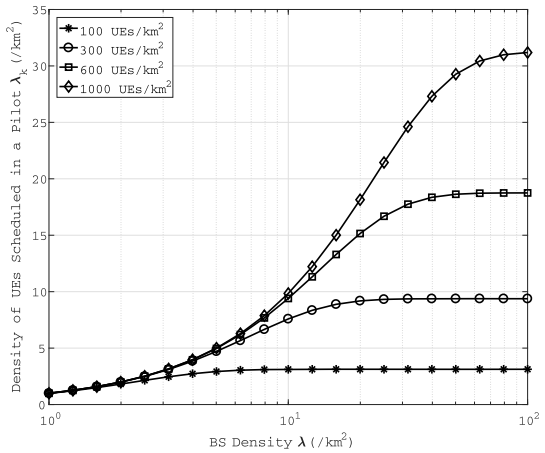

Fig. 3. Density of scheduled UEs in the same pilot, λ_k, vs the BS density, λ, with different UE density, ρ.

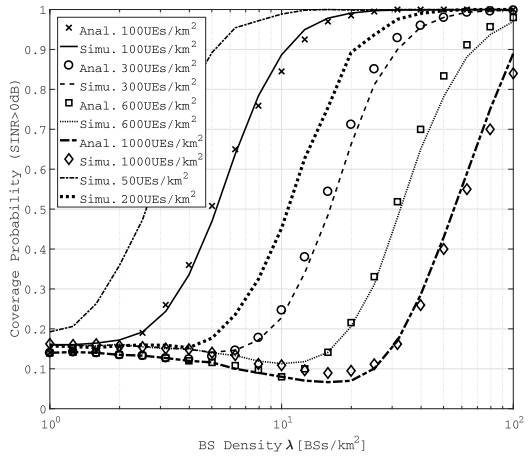

Fig. 4. The UL coverage probability vs. BS density.

A. UL Performance Analysis

In Fig. 4, we plot the UL coverage probability with respect to the BS density, λ, for various UE densities, ρ. From this figure, we can infer that

- There is a small gap between the numerical and the simulation results, mainly caused by the approximation in the derivations of the SINR, especially in the interference.
- When the BS deployment is sparse, the UL coverage probability is low, around 0.15. There is an UL coverage problem. The network is not properly dimensioned, and the available UL transmit power at the UE is not enough to reach the serving BS.
- When the BS density increases, the spatial reuse increases, and thus the number of simultaneously transmitting UEs and interference sources. Moreover, transmitting UEs get closer to their neighbouring BSs, with the consequent increase of both the pilot contamination and the received UL interference plus noise power. Moreover, some interferers transit from NLoS to LoS. As a result, there is a BS density regime in which the UL coverage probability suffers a decrease with the increase of the BS density. This decrease is more noticeable for larger UE densities.

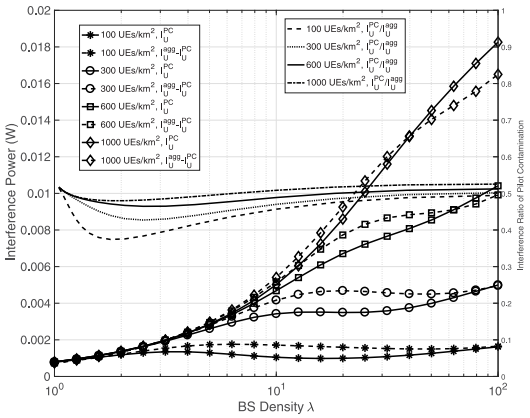

Fig. 5. The UL interference components vs. BS density.

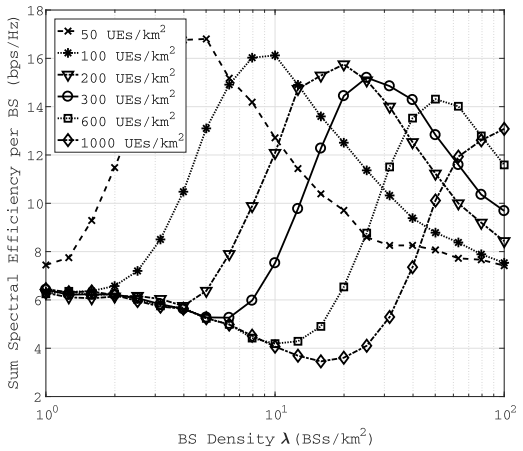

Fig. 6. The UL sum spectral efficiency per BS vs. BS density.

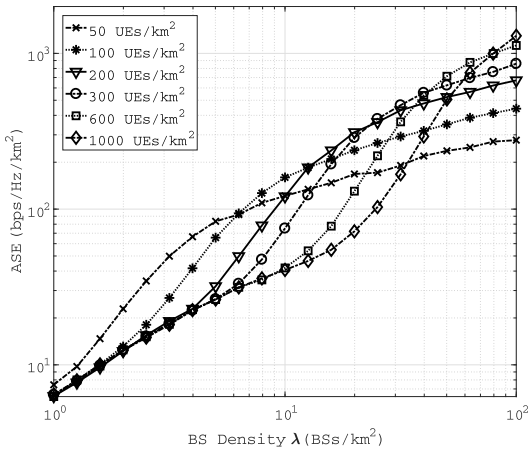

Fig. 7. The UL area spectral efficiency vs. BS density.

- When the BS density further increases, the number of simultaneously transmitting UEs and interference sources reaches its limit, as $\tilde{\rho}$ approaches ρ. Moreover, the number of UEs per BS decreases, which decreases the UL pilot reuse, and thus the pilot contamination. Since the signal power continues to increase as UEs get closer to their serving BSs with network densification, the UL coverage probability increases with it in this BS density regime.

It is important to note that since the signal power part is independent of the UE density, the former decrease and the later increase of the UL coverage probability mostly depends on the trend of interference power part, which will be analysed in the following. In Fig. 5, we plot the following 3 indicators 1) $\mathrm{I}_{\mathrm{U}}^{\mathrm{PC}}$, presented in (12), 2) $\mathrm{I}_{\mathrm{U}}^{\mathrm{agg}}$ - $\mathrm{I}_{\mathrm{U}}^{\mathrm{PC}}$, i.e. (13) minus (12), and 3) the ratio $\frac{\mathrm{I}_{\mathrm{U}}^{\mathrm{PC}}}{\mathrm{I}_{\mathrm{U}}^{\mathrm{agg}}}$, i.e. (12) divided by (13), with respect to the BS density, λ, for various UE densities, ρ. From this figure, we can see that

- The interference increases with respect to the BS density, following a very similar trend to the increase of the density of scheduled UEs using the same pilot, λ_k, in Fig. 3. This is because λ_k is a good measure of the number of simultaneously transmitting UEs and interference sources.
- When the BS density is much smaller than the UE density, the interference increases rapidly as all UL pilots are in use in all BSs.
- When the BS density is similar to or larger than the UE density, the increase of interference slows down, especially when λ_k reaches its maximum, indicating that all interference sources are on, and densification does not bring further spatial reuse.
- The interference power in the scenarios with a larger UE density is much stronger than that with a smaller one. The larger $\tilde{\rho}$, the larger λ_k, thus having more interference sources, which is inline with Remark 6. Moreover, the denser the interference sources, the larger the probability of LoS interference, which further aggravates the interference.
- Finally, note that the interference resulting from $\mathrm{I}_{\mathrm{U}}^{\mathrm{PC}}$ in (12) brings nearly the half of the overall interference in all scenarios, indicating the severity of the pilot contamination. Importantly, this ratio almost remains stable with the growth of the BS density, with a slight increase for the larger UE density. This indicates that the larger number of interference sources with the BS density is compensated by the less UL pilot reuse.

In Fig. 6, we plot the sum spectral efficiency per BS with respect to the BS density, λ, for various UE densities, ρ. Form this figure, we can observe that the sum spectral efficiency per BS starts at a given value, then decreases with the increase of the BS density, subsequently increases, and finally decreases. The first decrease and subsequent increase follows from the UL coverage probability behaviour, and thus we refer the reader to previous explanations. The final decrease, however, is driven by the number of UEs per BS. Since the sum spectral efficiency per BS is the sum of the spectral efficiencies of all UEs within a BS, it highly depends on the average number of UEs per BS. When the BS density is large enough, and the average BS load decrease, then the sum spectral efficiency per BS decreases too. As a result, we can conclude that exists an optimal BS density to maximise the sum spectral efficiency per BS, given a UE density. Likewise, there exists an optimal UE density to maximise the sum spectral efficiency per BS, for a given BS density. Such optimal solutions capitalise on striking the right balance between the signal quality and the BS load.

In Fig. 7, we also plot the ASE—the product of the BS density and the sum spectral efficiency per BS,

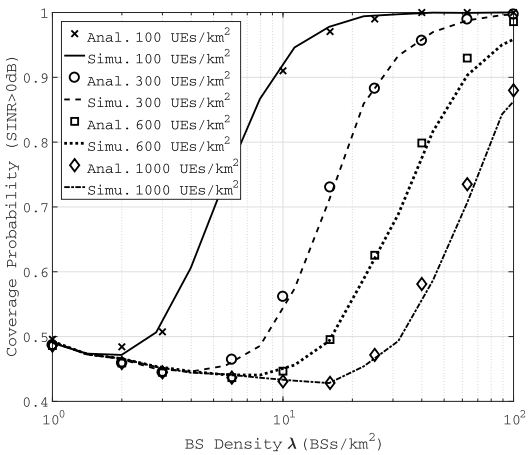

Fig. 8. The DL coverage probability vs. BS density.

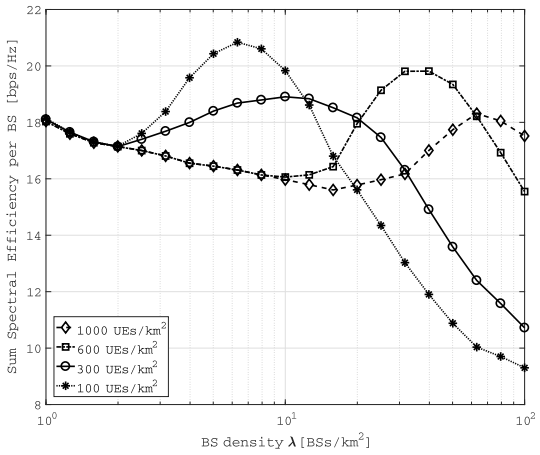

Fig. 9. The DL sum spectral efficiency per cell vs. BS density.

see (19)—with respect to the BS density, λ, for various UE densities, ρ, to show the overall mMIMO system capacity. From the figure, we can observe that a larger BS density generally results in a higher ASE. However, the ASE is not linearly increasing with the BS density. The ASE grows faster when the sum spectral efficiency per BS increases, and slows down with its decrease. Such slow down of ASE indicates that since the UE density is finite, at some point, increasing the BS density further does not introduce more spatial reuse. The denser the network the better, but there exits the risk of underutilising the deployed resources, and thus enter a non-cost-effective regime, a place where an operator does not want to be.

Importantly, we should highlight that the results in Fig. 7 show that there exists an optimal UE density to maximise the ASE, for a given BS density. For example, for a BS density of 10, 20, 50 and 100 BS/km^2, the best UE density is 100, 300, 600 and 1000 UE/km^2, respectively. This motivates the importance of **the UE scheduling problem** presented in (20).

B. DL Performance Analysis

In Fig. 8, the DL coverage probability with a SINR threshold of 0dB is plotted, and the following observations are done:

- The DL coverage probability shows a similar trend that the UL one. For brevity, we omit the detail explanations here. However, it is important to note that there is also a small gap between the numerical and the simulation results, caused by the approximation in the derivations of the SINR, especially in the interference.
- Different from the UL coverage probability, when the BS deployment is sparse, the DL one is larger, around 0.45. The main reasons are the larger DL transmission power at the BS and the lower number of interference sources. There are much less BS than UEs.

In Fig. 9, the DL sum spectral efficiency per BS is plotted, from which we can observe that 1) The DL sum spectral efficiency per BS shows a similar trend that the UL one. For brevity, we omit the detail explanation here. 2) Different for the UL coverage probability, larger efficiencies are achieved. This is due to the larger DL SINRs, which are reflected in the larger DL coverage probability. 3) Also note that an optimal BS density for a given UE density and an optimal UE density for a given BS density exist, which maximise the sum spectral efficiency per BS.

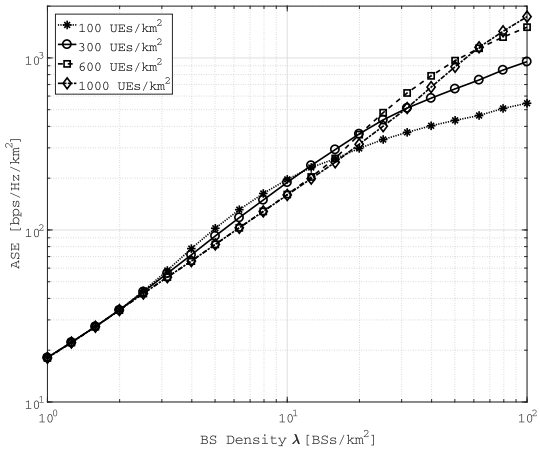

Fig. 10. The DL ASE vs. BS density.

In Fig. 10, the DL ASE is plotted, and we can see that

- Due to the larger SINRs, the ASE generally increases with the BS density.
- When the BS density is sparse, the ASE increases almost linearly with the BS density due to the high SINRs, despite of the initial decrease of the sum spectral efficiency per BS.
- When the BS density is denser, the ASE growth slows down as a result of the significant decrease of the sum spectral efficiency per BS, caused by the less number of UE per BS. This indicates that the spatial multiplexing capabilities of mMIMO are not fully used in each cell, It is also important to note that the increased number of BSs makes the interference severer, as *i)* the DL transmit power does not decrease with the BS density (no power control), and *ii)* the idle mode capability of BSs does not play a significant role at this BS densities.

C. Optimal Scheduling Problems

In Fig. 11, the impact of the UE density on the ASE performance is plotted, with $K_{\mathrm{T}} = 32$. From the figure, it can be seen that a larger BS density leads to a larger

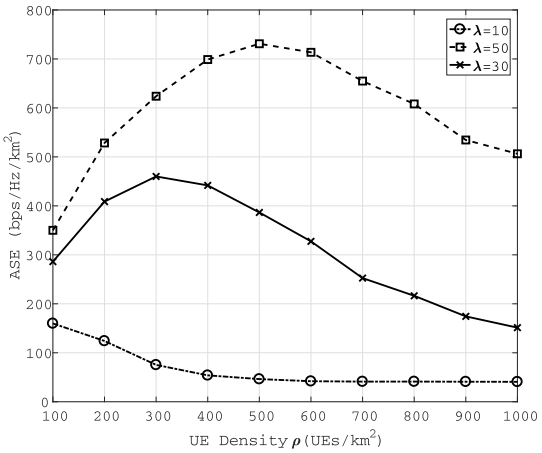

Fig. 11. The UL area spectral efficiency vs. UE densities.

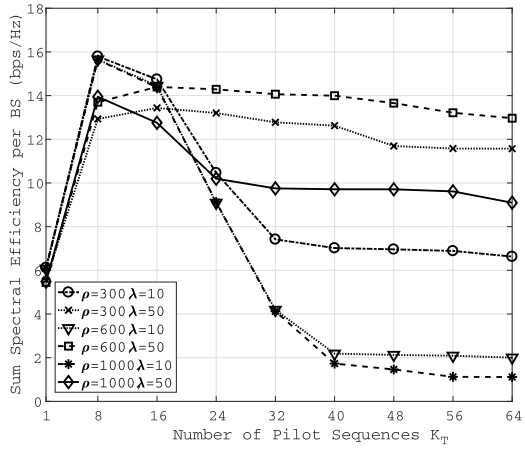

Fig. 12. The UL sum spectral efficiency vs. the number of pilots.

area spectral efficiency due to the more radio resources in a unit area. More importantly, as we proved and highlighted in Remark 11, the ASE is not a monotonically increasing with the growth of UE densities, which justifies the UE scheduling problem. In the scenario with the BS density $\lambda = 50\,\text{BS/km}^2$, when the UE density ρ grows from 100 to $500\,\text{UE/km}^2$, the ASE increases due to more UEs benefiting from the spatial reuse provided by MIMO systems. However, when ρ increases further, the ASE performance rapidly degrades. This is due to the increase of the aggregated interference —and especially the pilot contamination— caused by the more UEs in a unit area sharing the same pilot. In the scenario with the BS density $\lambda = 30\,\text{BS/km}^2$, a similar trend applies, and the only difference is that the inflexion point locates at $\rho = 300\,\text{UE/km}^2$. For the scenario with $\lambda = 10\,\text{BS/km}^2$, the ASE decreases as ρ grows from $100\,\text{UE/km}^2$ onwards. The increase region of ASE appears in the scenarios with a smaller density than $\rho = 100\,\text{UE/km}^2$, since the ASE equals to 0 with $\rho = 0\,\text{UE/km}^2$. From these two curves we can see that, a medium or slightly low load contributes to a larger ASE performance.

In Fig 12, different numbers of UL pilots, K_{T}, are investigated to show its performance impact on the UL sum spectral efficiency per BS. From the figure, we can see the concavity of the curves with respect to the number of UL pilots, K_{T}, as proved in the previous section. This justifies the UL pilot scheduling problem. Firstly, in those scenarios where the BS density is very sparse compared to the UE density, for instance, the scenarios represented by the pair (ρ, λ) with values $(300, 10)$, $(600, 10)$, $(1000, 10)$ and $(1000, 50)$, the sum spectral efficiency first increases with the growth of K_{T}, and then decreases with it. The reason behind this decrease in these high-loaded scenarios is that a larger K_{T} leads to a rapid increase of the density of simultaneously transmitting UEs, $\tilde{\rho}$, and thus a dramatic growth of the aggregated interference. Together with the high pilot overhead caused by the larger K_{T}, the sum spectral efficiency decreases fast until $\tilde{\rho}$ stops increasing. After that, the pilot contamination decreases with the further increase of K_{T}, but the pilot overhead still keeps increases, which together leads to a relatively stable performance. The smaller this UE-to-BS density ratio, the better performance in the stable region. In contrast, in the light-loaded scenarios, the decrease of sum spectral efficiency is not obvious. Although the pilot payload increases with K_{T}, the relief of pilot contamination due to the large K_{T} contributes to a better SINR performance.

Moreover, from all these curves, we can see that the optimal K_{T} tends to keep the network operating with a relative low $\tilde{\rho}$ to control the increase of the aggregated interference. Also, because of the overhead incurred by the UL pilot signal resource reservation, a large K_{T} is generally not a good choice. From the figure, the optimal values of K_{T} for these 6 scenarios are 8 and 16.

VII. Conclusion

In this paper, the UL and the DL performance of a multi-user mMIMO network is theoretically analysed using stochastic geometry, where a practical system model is embraced, including *i)* a finite UE density, *ii)* a path loss model, which differentiates LoS and NLoS channels, *iii)* a partical UL pilot to UE assignment, *iv)* the impact of pilot contamination, and *v)* an idle mode capability at the BSs. The coverage probability, per-BS spectral efficiency and network ASE are derived, after quantifying both the density of interfering sources in the UL and the DL, as well as the UL pilot contamination effect. Our results show that *i)* the UL and the DL SINRs significantly suffer in sparse networks with heavy-loads due to the severe pilot contamination and interference, and that *ii)* network densification reduces the number of UE per BS, and thus lead to a less aggressive UL pilot reuse, which significantly reduces the UL pilot contamination and enhances performance. Moreover, the performance impact of the scheduled UE density and the number of UL pilots are investigated, and optimal scheduling strategies to maximise the network performance are proposed.

Appendix A
Proof of Theorem 1

Firstly, the received UL signal power can be calculated as

$$P_0|\mathbf{g}_0^{\mathrm{H}}\bar{\mathbf{h}}_0|^2 = P_0|\mathbf{g}_0^{\mathrm{H}}\eta_0\mathbf{g}_0^*|^2 = P_0\eta_0^2|\mathbf{g}_0^*|^4 \overset{(a)}{\approx} P_0\eta_0^2\mathbb{E}\left[|\mathbf{g}_0^*|^4\right] = \begin{cases} P_u^2\left(M^2+M\right)\left(\zeta^{\mathrm{L}}(r)\right)^{2(1-\epsilon)}, & \text{w. } f_R^{\mathrm{L}}(r) \\ P_u^2\left(M^2+M\right)\left(\zeta^{\mathrm{NL}}(r)\right)^{2(1-\epsilon)}, & \text{w. } f_R^{\mathrm{NL}}(r). \end{cases} \tag{22}$$

where (a) uses the approximation $|\mathbf{g}_0^*|^4 \overset{M\to\infty}{\to} \mathbb{E}\left[|\mathbf{g}_0^*|^4\right]$, where the approximation error decays as $1/M^2$ according to [30].

According to [9], for tractable computation and to decouple the correlated terms in the denominator of SINR, approximations are used on the interference terms by using the expectation of these out-of-cell interference. Thus, the interference related components can be derived as

$$\begin{aligned} I_{\mathrm{U}}^1 &= P_0\mathbb{E}\left[|\mathbf{g}_0^{\mathrm{H}}\hat{\mathbf{e}}_0|^2\right] \overset{(a)}{=} \frac{1}{M}P_0\mathbb{E}\left[|\mathbf{g}_0^{\mathrm{H}}|^2\right]\mathbb{E}\left[|\hat{\mathbf{e}}_0|^2\right] \\ &\overset{(b)}{=} \frac{1}{M}P_u\zeta_0^{-\epsilon}\zeta_0\left(\sum_{x_i\in\tilde{\Phi}_u^{(1)}/0}P_i\zeta_{i0}+\frac{\sigma^2}{\tau}\right)\mathbb{E}\left[|\mathbf{Z}|^2\right]\mathbb{E}\left[|\mathbf{Z}|^2\right] \\ &\overset{(c)}{\approx} MP_u^2\zeta_0^{1-\epsilon}\left(\mathbb{E}\left[\sum_{x_i\in\tilde{\Phi}_u^{(1)}\setminus x_0}\zeta_{i0}\zeta_i^{-\epsilon}\right]+\frac{\sigma^2}{P_u\tau}\right), \end{aligned} \tag{23}$$

where (a) uses the independence of the two random vector and the independence among the random elements in each random vector, (b) uses the Gaussian distribution of $\mathbf{g}_0^{\mathrm{H}}$ and $\hat{\mathbf{e}}_0$, where $\mathbf{Z}$ denotes the standard Gaussian random vector, and step (c) uses the expectation of these out-of-cell interference to approximate the value [9].

Similarly, the second and the third components of the interference plus noise, I_{U}^2 and I_{U}^3, can be calculated as follows. The second component, I_{U}^2, captures the intra-cell and inter-cell interference, resulting from all the other simultaneous UL data transmissions in the serving and the neighbouring cells, i.e. $\tilde{\Phi}_u\setminus x_0$.

$$\begin{aligned} I_{\mathrm{U}}^2 &= \sum_{x_i\in\tilde{\Phi}_u\setminus x_0}P_i\mathbb{E}_{\mathbf{w}_{i0}}\left[|\mathbf{g}_0^{\mathrm{H}}\mathbf{h}_{i0}|^2\right] \\ &= \sum_{x_i\in\tilde{\Phi}_u\setminus x_0}P_i\mathbb{E}\left[\left|\Big(\sum_{x_j\in\tilde{\Phi}_u^{(1)}}\sqrt{P_j}\mathbf{h}_{j0}^{\mathrm{T}}+\mathbf{n}_u^{\mathrm{T}}\Big)\mathbf{h}_{i0}\right|^2\right] \\ &= \sum_{x_i\in\tilde{\Phi}_u\setminus x_0}P_i\mathbb{E}\left[|\mathbf{n}_u^{\mathrm{T}}\mathbf{h}_{i0}|^2\right]+\sum_{x_i\in\tilde{\Phi}_u\setminus x_0}P_i\mathbb{E}\left[\sum_{x_j\in\tilde{\Phi}_u^{(1)}}P_j|\mathbf{h}_{j0}^{\mathrm{T}}\mathbf{h}_{i0}|^2\right] \\ &\overset{(a)}{\approx} MP_u^2\frac{\sigma^2}{\tau}\mathbb{E}\left[\sum_{x_i\in\tilde{\Phi}_u\setminus x_0}\zeta_{i0}\zeta_i^{-\epsilon}\right] \\ &\quad+M^2\ P_u^2\mathbb{E}\left[\sum_{x_j\in\tilde{\Phi}_u^{(1)}\setminus x_0}\zeta_{j0}^2\zeta_j^{-2\epsilon}\right] \\ &\quad+MP_u\mathbb{E}\left[\sum_{x_i\in\tilde{\Phi}_u\setminus x_0}\zeta_{i0}\zeta_i^{-\epsilon}\right] \\ &\quad\times\left(\zeta_0^{1-\epsilon}+\mathbb{E}\left[\sum_{x_j\in\tilde{\Phi}_u^{(1)}\setminus x_0}\zeta_{j0}\zeta_j^{-\epsilon}\right]\right), \end{aligned} \tag{24}$$

where step (a) uses the expectation to approximate the value, as mentioned before, $\mathbb{E}\left[|\mathbf{h}_{j0}^{\mathrm{T}}\mathbf{h}_{i0}|^2\right]=\zeta_{j0}\zeta_{i0}M$, when $j\neq i$ due to the independence, and $\mathbb{E}\left[|\mathbf{h}_{j0}|^4\right]=(\zeta_{i0})^2(M^2+M)$, whose derivations are similar to Eq. (22), and step (b) in Eq. (23).

The third component I_{U}^3 captures the UL channel noise.

$$\begin{aligned} I_{\mathrm{U}}^3 &= \mathbb{E}\left[|\mathbf{g}_0^{\mathrm{H}}|^2\right]\sigma^2=\left(\sum_{x_i\in\tilde{\Phi}_u^{(1)}}P_i\zeta_{i0}+\frac{\sigma^2}{\tau}\right)\mathbb{E}\left[|\mathbf{Z}|^2\right]\sigma^2 \\ &= P_uM\sigma^2\left(\zeta_0^{1-\epsilon}+\mathbb{E}\left[\sum_{i\in\tilde{\Phi}_u^{(1)}\setminus x_0}\zeta_{i0}\left(\zeta_i\right)^{-\epsilon}\right]+\frac{\sigma^2}{P_u\tau}\right). \end{aligned} \tag{25}$$

For the calculation of interference, two auxiliary functions are introduced. Firstly, the pilot contamination-related function to calculate the following expectation.

$$\begin{aligned} &\mathbb{E}\left[\sum_{x_i\in\tilde{\Phi}_u^{(1)}\setminus x_0}\left(\zeta_{i0}\zeta_i^{-\epsilon}\right)^a\right] \\ &\overset{(a)}{=} 2\pi\rho_1(x)\int_0^\infty(\zeta(x))^a\left[\int_0^{x'}(\zeta(u))^{-a\epsilon}f_{R|x}(u)\mathrm{d}u\right]x\mathrm{d}x \\ &\overset{(b)}{=} 2\pi\lambda_1\int_0^\infty\left(1-\exp\left(-\frac{12}{5}\lambda_1\pi x^2\right)\right)\times\Bigg((\zeta^{\mathrm{L}}(x))^a\mathrm{Pr}^{\mathrm{L}}(x) \\ &\quad\times\Big[\int_0^x\left(\zeta^{\mathrm{L}}(u)\right)^{-a\epsilon}f_R^{\mathrm{L}}(u)\mathrm{d}u+\int_0^{x_1}\left(\zeta^{\mathrm{NL}}(u)\right)^{-a\epsilon}f_R^{\mathrm{NL}}(u)\mathrm{d}u\Big] \\ &\quad+(\zeta^{\mathrm{NL}}(x))^a\mathrm{Pr}^{\mathrm{NL}}(x)\Big[\int_0^{x_2}\left(\zeta^{\mathrm{L}}(u)\right)^{-a\epsilon}f_R^{\mathrm{L}}(u)\mathrm{d}u \\ &\quad+\int_0^x\left(\zeta^{\mathrm{NL}}(u)\right)^{-a\epsilon}f_R^{\mathrm{NL}}(u)\mathrm{d}u\Big]\Bigg)\mathrm{d}x\triangleq\mathrm{A}^a(\lambda_1) \end{aligned} \tag{26}$$

where step (a) uses notation change, $D_{i0}=x$, and the maximum received power association, $\zeta(x)<\zeta(u)$, and step (b) uses the density function, $\rho_1(x)$, presented in (9), and $x_1=\arg\limits_{x_1}\left\{\zeta^{\mathrm{NL}}(x_1)=\zeta^{\mathrm{L}}(x)\right\}$ and $x_2=\arg\limits_{x_2}\left\{\zeta^{\mathrm{L}}(x_2)=\zeta^{\mathrm{NL}}(x)\right\}$. Moreover, the interference related function is introduced as follows.

$$\begin{aligned} &\mathbb{E}\left[\sum_{x_i\in\tilde{\Phi}_u\setminus x_0}\zeta_{i0}(\zeta_i)^{-\epsilon}\right] \\ &=2\pi\tilde{\rho}\int_0^\infty\zeta(x)\Big(\int_0^{x'}(\zeta(u))^{-\epsilon}f_{R|x}(u)\mathrm{d}u\Big)x\mathrm{d}x\triangleq\mathrm{B}(\tilde{\rho}) \\ &=2\pi\tilde{\rho}\int_0^\infty\zeta(x)\Bigg((\zeta^{\mathrm{L}}(x))^a\mathrm{Pr}^{\mathrm{L}}(x)\Big[\int_0^x\left(\zeta^{\mathrm{L}}(u)\right)^{-a\epsilon}f_R^{\mathrm{L}}(u)\mathrm{d}u \\ &\quad+\int_0^{x_1}\left(\zeta^{\mathrm{NL}}(u)\right)^{-a\epsilon}f_R^{\mathrm{NL}}(u)\mathrm{d}u\Big]+(\zeta^{\mathrm{NL}}(x))^a\mathrm{Pr}^{\mathrm{NL}}(x) \\ &\quad\times\Big[\int_0^{x_2}\left(\zeta^{\mathrm{L}}(u)\right)^{-a\epsilon}f_R^{\mathrm{L}}(u)\mathrm{d}u+\int_0^x\left(\zeta^{\mathrm{NL}}(u)\right)^{-a\epsilon}f_R^{\mathrm{NL}}(u)\mathrm{d}u\Big]\Bigg)\mathrm{d}x \end{aligned} \tag{27}$$

APPENDIX B
PROOF OF THEOREM 2

To simplify the formulation of the SINR, a normalising factor, $\frac{1}{\kappa_0^2\eta_0^2}$, is used in both the numerator and the denominator of the DL SINR. Similar to the signal part of the UL SINR,

we have that

$$\frac{1}{\kappa_0^2\eta_0^2}P_d|\bar{\mathbf{h}}_0^{\mathrm{H}}\mathbf{u}_0|^2 = \begin{cases} P_dP_u\left(M^2+M\right)\left(\zeta^{\mathrm{L}}(r)\right)^{2-\varepsilon} & \text{w.}f_R^{\mathrm{L}}(r) \\ P_dP_u\left(M^2+M\right)\left(\zeta^{\mathrm{NL}}(r)\right)^{2-\varepsilon} & \text{w.}f_R^{\mathrm{NL}}(r) \end{cases}$$

The first scaled component of denominator captures the interference introduced by the wanted signal as a result of the misalignment of the precoding vector due to channel estimation error.

$$\begin{aligned}\frac{I_{\mathrm{D}}^1}{\kappa_0^2\eta_0^2} &= \frac{P_d\mathbb{E}_{\hat{\mathbf{e}}_0}\left[|\hat{\mathbf{e}}_0^{\mathrm{H}}\mathbf{u}_0|^2\right]}{\kappa_0^2\eta_0^2} \overset{(a)}{=} \frac{P_d}{\kappa_0^2\eta_0^2}\frac{1}{M}\mathbb{E}\left[|\hat{\mathbf{e}}_0^{\mathrm{H}}|^2\right]\mathbb{E}\left[|\mathbf{u}_0|^2\right] \\ &\overset{(b)}{=} \frac{P_d}{M}\zeta_0\left(\sum_{x_i\in\tilde{\Phi}_u^{(1)}\setminus x_0}P_i\zeta_{i0}+\frac{\sigma^2}{\tau}\right)\mathbb{E}\left[|\mathbf{Z}|^2\right]\mathbb{E}\left[|\mathbf{Z}|^2\right] \\ &\overset{(c)}{\approx} MP_dP_u\zeta_0\left(\mathbb{E}\left[\sum_{x_i\in\tilde{\Phi}_u^{(1)}\setminus x_0}\zeta_{i0}\left(\zeta_i\right)^{-\epsilon}\right]+\frac{\sigma^2}{P_u\tau}\right)\end{aligned}$$

where (a), (b) and (c) are the same as those in I_{U}^1.

The second component captures the intra-cell and inter-cell interference, resulting from all the other simultaneous DL data transmissions in the serving and the neighbouring cells, i.e. $\tilde{\Phi}_b\setminus x_0$.

$$\begin{aligned}\frac{I_{\mathrm{D}}^2}{\kappa_0^2\eta_0^2} &= P_d\sum_{k=1}^{K_{\mathrm{T}}}\sum_{\substack{y_j\in\tilde{\Phi}_b^{(k)}\\ x_i\in V(y_j)\\ x_i\neq x_0}}\mathbb{E}\left[\frac{\kappa_i^2\eta_i^2}{\kappa_0^2\eta_0^2}|\mathbf{h}_{0j}^{\mathrm{H}}\mathbf{n}_{\mathbf{u}}+\sum_{x_n\in\tilde{\Phi}_u^{(k)}}\sqrt{P_n}\mathbf{h}_{0j}^{\mathrm{H}}\mathbf{h}_{nj}|^2\right] \\ &\overset{(a)}{\approx} P_d\left(\sum_{y_j\in\tilde{\Phi}_b}\zeta_{0j}M\frac{\sigma^2}{\tau}+\sum_{x_n\in\tilde{\Phi}_u}P_n\mathbb{E}\left[|\mathbf{h}_{0j}^{\mathrm{H}}\mathbf{h}_{nj}|^2\right]\right) \\ &\overset{(b)}{\approx} MP_d\frac{\sigma^2}{\tau}\mathbb{E}\left[\sum_{y_j\in\tilde{\Phi}_b\setminus y_0}\zeta_{0j}\right] \\ &\quad + M^2\ P_uP_d\zeta_0^{-\epsilon}\mathbb{E}\left[\sum_{y_j\in\Phi_b^{(1)}\setminus y_0}\left(\zeta_{0j}\right)^2\right] \\ &\quad + M\ P_uP_d\mathbb{E}\left[\sum_{y_j\in\tilde{\Phi}_b\setminus y_0}\zeta_{0j}\right]\mathbb{E}\left[\sum_{x_n\in\tilde{\Phi}_u\setminus x_0}\zeta_{nj}\left(\zeta_n\right)^{-\epsilon}\right]\end{aligned}$$

where step (a) uses $\mathbb{E}\frac{\kappa_i^2\eta_i^2}{\kappa_0^2\eta_0^2}\approx 1$, and step (b) follows assuming that the distances D_{0j} and D_{nj} are independent, Moreover, the second item after step (b) follows by focusing on $k=1$ and $n=0$, i.e. the pilot contamination in the precoding matrix caused by the typical UE to other UEs allocated with the same pilot, the first pilot.

The third component captures the DL channel noise, which is given by

$$\begin{aligned}\frac{I_{\mathrm{D}}^3}{\kappa_{0,10}^2\eta_{0,10}^2} &= \sigma^2\mathbb{E}\left[N_0\right]\left(P_u\mathbb{E}\left[\sum_{x_i\in\tilde{\Phi}_u^{(1)}}\zeta_{i0}\left(\zeta_i\right)^{-\epsilon}\right]+\frac{\sigma^2}{\tau}\right) \\ &= \sigma^2\bar{N}\left(P_u\mathrm{A}(\lambda_1)+\frac{\sigma^2}{\tau}\right).\end{aligned}$$

To calculate the DL interference-related expectation, the following auxiliary function is introduced.

$$\begin{aligned}\mathrm{C}^a(b) &= \mathbb{E}\left[\sum_{j\in\Psi\setminus o}\left(\zeta_{0j}\right)^a\right] \\ &\overset{(a)}{=} \begin{cases} 2\pi b\Big(\int_r^\infty\left(\zeta^{\mathrm{L}}(x)\right)^a\Pr{}^{\mathrm{L}}(x)x\mathrm{d}x \\ \qquad +\int_{r_1}^\infty\left(\zeta^{\mathrm{NL}}(x)\right)^a\Pr{}^{\mathrm{NL}}(x)x\mathrm{d}x\Big) \\ 2\pi b\Big(\int_{r_2}^\infty\left(\zeta^{\mathrm{L}}(x)\right)^a\Pr{}^{\mathrm{L}}(x)x\mathrm{d}x \\ \qquad +\int_r^\infty\left(\zeta^{\mathrm{NL}}(x)\right)^a\Pr{}^{\mathrm{NL}}(x)x\mathrm{d}x\Big) \end{cases}\end{aligned} \tag{28}$$

where (a) considers the LoS/NLoS signal with the serving distance r and the association criterion $\zeta_{0j}<\zeta_0$, and b denotes the density of the HPPP Ψ.

Substituting the auxiliary functions $A(\cdot)$, $B(\cdot)$ and $C(\cdot)$, the interference plus noise can be represented by these auxiliary functions. Proof completes.

APPENDIX C
PROOF OF LEMMA 1

The conclusion that $\tilde{\rho}$ is concave downward with respect to ρ can be achieved by the following steps:

- The active UE density, $\tilde{\rho}$, is a monotonically increasing function of the UE density, ρ, and approaches a maximum value, $K_{\mathrm{T}}\lambda$ (see in Section III),
- With a relative small UE density, ρ, the active UE density, $\tilde{\rho}$, equasl the UE density, $\tilde{\rho}=\rho$, because the service limit caused by K_{T} can be neglected, and all UEs can be served. Thus, we have that $\frac{\partial\tilde{\rho}}{\partial\rho}|_{\rho\to 0}=1$.
- The growth of the UE density, ρ, increases the probability that there are more than K_{T} UEs in one active cell. Given a pilot number, K_{T}, we have that $\bar{N}<\frac{\varrho}{\lambda}$, where $\frac{\varrho}{\lambda}$ is the mean value of the negative binomial distribution without the upper limit, K_{T}. Thus, the slope of the active UE density, $\tilde{\rho}$, with the UE density, ρ, is less than 1. The further increase of the UE density, ρ, leads to the more cells with a number of UE larger than K_{T}, the growth of the active UE density, $\tilde{\rho}$, thus slows down.
- Due to the limitation of the active UE density, $\tilde{\rho}$, which is independent of the UE density, ρ, with a very large UE density, ρ, we have that $\frac{\partial\tilde{\rho}}{\partial\rho}|_{\rho\gg K_{\mathrm{T}}\lambda}=0$.

APPENDIX D
PROOF OF LEMMA 2

Firstly, we divide the ASE function with the UE density, ρ, into two composition functions: $\mathrm{ASE}(\tilde{\rho})$ and $\tilde{\rho}(\rho)$, where the latter is proved to be a concave function with respect to the UE density, ρ. Thus, the ASE is concave with respect to the UE density, ρ, if the ASE is concave and increasing with respect to the active UE density, $\tilde{\rho}$.

Secondly, we rewrite the formulation of the ASE with respect to $\tilde{\rho}$ given $\lambda_k=0$ and $\sigma=0$, that is, $\mathrm{ASE}(\tilde{\rho})=\tilde{\rho}\log\left(1+\mathrm{S/I}(\tilde{\rho})\right)$, where $I(\tilde{\rho})=a\tilde{\rho}$ according to (22), and a is a factor independent of ρ. So we can simplify

the formulation of $\mathrm{ASE}(\tilde{\rho})$ as a general function, $y(x) = x\log(1+c/x)$, where $c>0$.

Thirdly, we can prove that $y(x)$ is an increasing function, since $y'(x) = \log(1+c/x) - c/(c+x) \geq 0$ according to the inequality, $\log(1+x) \geq \frac{x}{1+x}$. Furthermore, we have that $y''(x) = -\frac{c^2}{(x+c)^2\, x} < 0$. Hence, it is a concave downward function.

The proof completes.

Appendix E
Proof of Theorem 3

According to the interference formulation (12), considering the impact of pilot contamination, different with the above cases, we have that $I(\tilde{\rho}) = a\tilde{\rho}^2 + b\tilde{\rho}$, because the density $\lambda_k = \frac{1}{K_\mathrm{T}}\tilde{\rho}$. Then, we focus on the first derivative of $\mathrm{ASE}(\rho)$, that is, $\mathrm{ASE}'(\rho) = \frac{\partial \mathrm{ASE}}{\partial \tilde{\rho}}\frac{\partial \tilde{\rho}}{\partial \rho}$. Note that, according to Lemma 1, we have that $\tilde{\rho}'(\rho) > 0$.

Hence, we have the formulation $\mathrm{ASE}(\tilde{\rho}) = \tilde{\rho}\log(1+\frac{\mathrm{S}}{\mathrm{a}\tilde{\rho}^2+\mathrm{b}\tilde{\rho}})$, where $a>0$ and $b>0$. Its first derivative is given as $\log(1+\frac{S}{I}) - \frac{S}{I}\frac{I+a\tilde{\rho}^2}{I+S}$. According to the inequality, $\log(1+x) \leq x$, we can conclude that if $a\tilde{\rho}^2 > S$, then $\frac{I+a\tilde{\rho}^2}{I+S} > 1$, and thus $\mathrm{ASE}'(\tilde{\rho}) < 0$. This means the ASE decreases with $\tilde{\rho}$ in such cases.

Specifically, when ρ grows from 0 to ∞, $\tilde{\rho}$ grows from 0 to $K_\mathrm{T}\lambda$, while S depends on the BS density, λ, which is a constant independent with ρ. Once $a\tilde{\rho}^2 > S$, the ASE starts to decrease, which depends on the BS density λ and pilot number K_T. In a sparse network with a low density of BSs, where the signal part S is relative small due to the long serving distance, this phenomena comes earlier with the growth of ρ.

Moreover, it is obvious that $\lim_{\rho\to 0}\mathrm{ASE} = 0$. Thus the ASE increases first when ρ grows from a small value. Integrating the two trends of the ASE, the proof completes.

Appendix F
Proof of Theorem 4

Under the scenario $\rho \gg K_\mathrm{T}$, we have the following limits: $\tilde{\rho} \approx K_\mathrm{T}\lambda$, $\bar{N} \approx K_\mathrm{T}$ and $\lambda_k \approx \lambda$. Thus, based on the formulation of UL interference, we can have the following simplified expression: $I(K_\mathrm{T}) = aK_\mathrm{T}$, and $\mathrm{S}(K_\mathrm{T}) = (1-cK_\mathrm{T})K_\mathrm{T}\log(1+\frac{s}{aK_\mathrm{T}})$, where $0 < c < 1/K_\mathrm{T}$ ensures the efficiency factor is between $(0,1)$.

From this formulation, we can obtain the second derivative of the sum spectrum efficiency, $\mathrm{S}''(K_\mathrm{T})$. That is,

$$\mathrm{S}'' = -2c\log(1+\frac{s}{aK_\mathrm{T}}) + \frac{s}{aK_\mathrm{T}}\frac{c(K_\mathrm{T}+1)}{K_\mathrm{T}+\frac{s}{a}} - \frac{s^2}{a^2}\frac{1-cK_\mathrm{T}}{K_\mathrm{T}(K_\mathrm{T}+\frac{s}{a})^2}.$$

Substituting $\log(1+\frac{s}{aK_\mathrm{T}})$ with its lower limit $\frac{\frac{s}{a}}{K_\mathrm{T}+\frac{s}{a}}$, we have that

$$-2c\log(1+\frac{s}{aK_\mathrm{T}}) + \frac{s}{aK_\mathrm{T}}\frac{c(K_\mathrm{T}+1)}{K_\mathrm{T}+\frac{s}{a}} \leq -2c\frac{\frac{s}{a}}{K_\mathrm{T}+\frac{s}{a}} + \frac{s}{aK_\mathrm{T}}\frac{c(K_\mathrm{T}+1)}{K_\mathrm{T}+\frac{s}{a}} = \frac{\frac{s}{a}c\left(\frac{1}{K_\mathrm{T}}-1\right)}{K_\mathrm{T}+\frac{s}{a}} < 0$$

Since the third item is less than 0, we can conclude that $\mathrm{S}'' < 0$.

References

[1] T. L. Marzetta, "Noncooperative cellular wireless with unlimited numbers of base station antennas," *IEEE Trans. Wireless Commun.*, vol. 9, no. 11, pp. 3590–3600, Nov. 2010.

[2] E. G. Larsson, O. Edfors, F. Tufvesson, and T. L. Marzetta, "Massive MIMO for next generation wireless systems," *IEEE Commun. Mag.*, vol. 52, no. 2, pp. 186–195, Feb. 2014.

[3] T. L. Marzetta, "How much training is required for multiuser MIMO?" in *Proc. Asilomar Conf. Signals, Syst. Comput. (ACSSC)*, Oct. 2006, pp. 359–363.

[4] J. Jose, A. Ashikhmin, T. L. Marzetta, and S. Vishwanath, "Pilot contamination and precoding in multi-cell TDD systems," *IEEE Trans. Wireless Commun.*, vol. 10, no. 8, pp. 2640–2651, Aug. 2011.

[5] J. Hoydis, S. ten Brink, and M. Debbah, "Massive MIMO in the UL/DL of cellular networks: How many antennas do we need?" *IEEE J. Sel. Areas Commun.*, vol. 31, no. 2, pp. 160–171, Feb. 2013.

[6] H. Q. Ngo, M. Matthaiou, T. Q. Duong, and E. G. Larsson, "Uplink performance analysis of multicell MU-SIMO systems with ZF receivers," *IEEE Trans. Veh. Technol.*, vol. 62, no. 9, pp. 4471–4483, Nov. 2013.

[7] M. Matthaiou, C. Zhong, M. R. McKay, and T. Ratnarajah, "Sum rate analysis of ZF receivers in distributed MIMO systems," *IEEE J. Sel. Areas Commun.*, vol. 31, no. 2, pp. 180–191, Feb. 2013.

[8] N. Krishnan, R. D. Yates, and N. B. Mandayam, "Uplink linear receivers for multi-cell multiuser MIMO with pilot contamination: Large system analysis," *IEEE Trans. Wireless Commun.*, vol. 13, no. 8, pp. 4360–4373, Aug. 2014.

[9] T. Bai and R. W. Heath, Jr., "Analyzing uplink SINR and rate in massive MIMO systems using stochastic geometry," *IEEE Trans. Commun.*, vol. 64, no. 11, pp. 4592–4606, Nov. 2016.

[10] Y. Saito, A. Benjebbour, A. Li, K. Takeda, Y. Kishiyama, and T. Nakamura, "System-level evaluation of downlink non-orthogonal multiple access (NOMA) for non-full buffer traffic model," in *Proc. IEEE Conf. Standards Commun. Netw. (CSCN)*, Oct. 2015, pp. 94–99.

[11] Q. Zhang, H. H. Yang, T. Q. S. Quek, and J. Lee, "Heterogeneous cellular networks with LoS and NLoS transmissions—The role of massive MIMO and small cells," *IEEE Trans. Wireless Commun.*, vol. 16, no. 12, pp. 7996–8010, Dec. 2017.

[12] E. Sadeghabadi, S. M. Azimi-Abarghouyi, B. Makki, M. Nasiri-Kenari, and T. Svensson, "Asynchronous downlink massive MIMO networks: A stochastic geometry approach," *IEEE Trans. Wireless Commun.*, vol. 19, no. 1, pp. 579–594, Jan. 2020.

[13] D. Verenzuela, E. Björnson, and L. Sanguinetti, "Spectral and energy efficiency of superimposed pilots in uplink massive MIMO," *IEEE Trans. Wireless Commun.*, vol. 17, no. 11, pp. 7099–7115, Nov. 2018.

[14] A. Papazafeiropoulos, P. Kourtessis, M. D. Renzo, S. Chatzinotas, and J. M. Senior, "Performance analysis of cell-free massive MIMO systems: A stochastic geometry approach," *IEEE Trans. Veh. Technol.*, vol. 69, no. 4, pp. 3523–3537, Apr. 2020.

[15] P. Parida and H. S. Dhillon, "Stochastic geometry-based uplink analysis of massive MIMO systems with fractional pilot reuse," *IEEE Trans. Wireless Commun.*, vol. 18, no. 3, pp. 1651–1668, Mar. 2019.

[16] *Further Advancements for E-UTRA Physical Layer Aspects*, document TR 36.814, 3GPP, Mar. 2017.

[17] S. Sesia, I. Toufik, and M. Baker, *LTE—The UMTS Long Term Evolution: From Theory to Practice*. Hoboken, NJ, USA: Wiley, 2011.

[18] W. Xiao, R. Ratasuk, A. Ghosh, R. Love, Y. Sun, and R. Nory, "Uplink power control, interference coordination and resource allocation for 3GPP E-UTRA," in *Proc. IEEE Veh. Technol. Conf.*, Sep. 2006, pp. 1–5.

[19] J. Mao, J. Gao, Y. Liu, and G. Xie, "Simplified semi-orthogonal user selection for MU-MIMO systems with ZFBF," *IEEE Wireless Commun. Lett.*, vol. 1, no. 1, pp. 42–45, Feb. 2012.

[20] M. Benmimoune, E. Driouch, W. Ajib, and D. Massicotte, "Joint transmit antenna selection and user scheduling for massive MIMO systems," in *Proc. IEEE Wireless Commun. Netw. Conf. (WCNC)*, Mar. 2015, pp. 381–386.

[21] M. Ding *et al.*, "Performance impact of LoS and NLoS transmissions in dense cellular networks," *IEEE Trans. Wireless Commun.*, vol. 15, no. 3, pp. 2365–2380, Mar. 2016.

[22] S. Lee and K. Huang, "Coverage and economy of cellular networks with many base stations," *IEEE Commun. Lett.*, vol. 16, no. 7, pp. 1038–1040, Jul. 2012.

[23] M. Ding, D. López-Pérez, G. Mao, and Z. Lin, "Performance impact of idle mode capability on dense small cell networks," *IEEE Trans. Veh. Technol.*, vol. 66, no. 11, pp. 10446–10460, Nov. 2017.
[24] Y. Chen, M. Ding, D. López-Pérez, Z. Lin, and G. Mao, "A space-time analysis of LTE and Wi-Fi inter-working," *IEEE J. Sel. Areas Commun.*, vol. 34, no. 11, pp. 2981–2998, Nov. 2016.
[25] C. Li, J. Zhang, and K. B. Letaief, "Throughput and energy efficiency analysis of small cell networks with multi-antenna base stations," *IEEE Trans. Wireless Commun.*, vol. 13, no. 5, pp. 2505–2517, May 2014.
[26] A. I. Aravanis, T. T. Lam, O. Muñoz, A. Pascual-Iserte, and M. D. Renzo, "A tractable closed form approximation of the ergodic rate in Poisson cellular networks," *EURASIP J. Wireless Commun. Netw.*, vol. 2019, no. 1, pp. 1651–1668, Dec. 2019.
[27] M. Haenggi, "User point processes in cellular networks," *IEEE Wireless Commun. Lett.*, vol. 6, no. 2, pp. 258–261, Apr. 2017.
[28] M. Ding, D. López-Pérez, G. Mao, P. Wang, and Z. Lin, "Will the area spectral efficiency monotonically grow as small cells go dense?" in *Proc. IEEE Globecom*, Dec. 2015, pp. 1–7.
[29] *Further Enhancements to LTE Time Division Duplex for Downlink-Uplink Interference Management and Traffic Adaptation*, document TR 36.828, 3GPP, Jun. 2012.
[30] H. Q. Ngo, E. G. Larsson, and T. L. Marzetta, "Aspects of favorable propagation in massive MIMO," in *Proc. 22nd Eur. Signal Process. Conf. (EUSIPCO)*, Sep. 2014, pp. 76–80.

Youjia Chen (Member, IEEE) received the B.S. and M.S. degrees in communication engineering from Nanjing University, China, in 2005 and 2008, respectively, and the Ph.D. degree in wireless engineering from The University of Sydney, Australia, in 2017. From 2008 to 2009, she was with Alcatel-Lucent Shanghai Bell, where she was involved in the development of core-network protocol stacks. She was a Lecture with the College of Photonic and Electrical Engineering, Fujian Normal University, China, in August 2009. In 2018, she joined the College of Physics and Information Engineering, Fuzhou University, as a Professor. Her research interests include ultra-dense networks, massive MIMO, wireless caching/computing, intelligent reflecting surfaces, and artificial intelligence in wireless resource allocation.

Ming Ding (Senior Member, IEEE) received the B.S. and M.S. degrees (Hons.) in electronics engineering and the Ph.D. degree in signal and information processing from Shanghai Jiao Tong University (SJTU), Shanghai, China, in 2004, 2007, and 2011, respectively. From April 2007 to September 2014, he worked at Sharp Laboratories of China, Shanghai, as a Researcher/Senior Researcher/Principal Researcher. He is currently a Senior Research Scientist at Data61, CSIRO, Sydney, NSW, Australia. He has authored over 140 papers in IEEE journals and conferences, all in recognized venues, and around 20 3GPP standardization contributions, as well as the book *Multi-point Cooperative Communication Systems: Theory and Applications* (Springer). He also holds 21 U.S. patents and co-invented more than 100 patents on 4G/5G technologies in CN, JP, KR, and EU. His research interests include information technology, data privacy and security, machine learning, and AI. He is currently an Editor of IEEE TRANSACTIONS ON WIRELESS COMMUNICATIONS and IEEE COMMUNICATIONS SURVEYS AND TUTORIALS. He has also served as a/the guest editor/co-chair/co-tutor/TPC member for many IEEE top-tier journals/conferences and received several awards for his research work and professional services.

David López-Pérez (Senior Member, IEEE) is an Expert and the Technical Leader of Huawei Paris Research Center, France, who has devoted most of his career to the study of both cellular and Wi-Fi networks, where his main research interests are in network performance analysis, both theoretical-based and simulation-based, network planning, and optimization, as well as technology and feature development. His main contributions are around the understanding of small cells and ultra-dense networks. He has also pioneered work on energy efficiency, cellular and Wi-Fi inter-working, and investigated both multi-antenna capabilities and ultra-reliable low latency features for future indoor networks. He was recognized as a Bell Labs Distinguished Member of Staff in 2019. He has authored one book on small cells and has published more than 150 research manuscripts on a variety of related topics. He has filed 54 patents applications with more than 25 granted as of today and has received a number of prestigious awards. He is an Editor of IEEE TRANSACTIONS ON WIRELESS COMMUNICATIONS.

Xuefeng Yao received the B.S. degree in electronics information science and technology from Jilin University, China, in 2015, and the M.S. degree in wireless engineering from The University of Sydney, Australia, in 2019. In 2019, he joined Baidu Inc., as an Engineer of Baidu's open source deep learning platform, PaddlePaddle. His research interests include ultra-dense networks, massive MIMO, and deep learning.

Zihuai Lin (Senior Member, IEEE) received the Ph.D. degree in electrical engineering from Chalmers University of Technology, Sweden, in 2006. Prior to this, he has held positions at Ericsson Research, Stockholm, Sweden. Following Ph.D. graduation, he worked as a Research Associate Professor at Aalborg University, Denmark. He is currently working at the School of Electrical and Information Engineering, The University of Sydney, Australia. His research interests include source/channel/network coding, coded modulation, MIMO, OFDMA, SC-FDMA, radio resource management, cooperative communications, small-cell networks, and 5G cellular systems.

Guoqiang Mao (Fellow, IEEE) is a Distinguished Professor and the Dean of the Research Institute of Smart Transportation, Xidian University. Prior to this, he was with the University of Technology Sydney and The University of Sydney. He has published over 200 papers in international conferences and journals that have been cited more than 10 000 times. His research interests include intelligent transport systems, the Internet of Things, wireless localization techniques, wireless sensor networks, and applied graph theory and its applications in telecommunications. He is a fellow of IET. He received the Top Editor Award for his outstanding contributions to the IEEE TRANSACTIONS ON VEHICULAR TECHNOLOGY in 2011, 2014, and 2015. He was the Co-Chair of IEEE Intelligent Transport Systems Society Technical Committee on Communication Networks. He has served as the chair, the co-chair, and a TPC member in a number of international conferences. He was an Editor of IEEE TRANSACTIONS ON WIRELESS COMMUNICATIONS from 2014 to 2019 and IEEE TRANSACTIONS ON VEHICULAR TECHNOLOGY from 2010 to 2020. He has been an Editor of the IEEE TRANSACTIONS ON INTELLIGENT TRANSPORTATION SYSTEMS since 2018.